Department of Physics and Astronomy
University of Heidelberg

Bachelor thesis
in Physics
submitted by

Auguste Henriette Schulz

born in Munich

2015

Jet cross sections and properties in proton-proton collisions at $\sqrt{s} = 7$ TeV analysed within the C++ framework Rivet

This bachelor thesis has been carried out by
Auguste Henriette Schulz
at the Physikalisches Institut Heidelberg
under the supervision of
Prof. Dr. Johanna Stachel

Abstract:

Based on the implementation of a jet analysis [1] of the ALICE Collaboration in the Rivet framework, a Monte Carlo study is carried out. The analysis is concerned with charged jet cross sections, jet fragmentation distributions, multiplicities and observables measuring the spatial extent of jets. They are measured in proton-proton collisions at $\sqrt{s}$ =7 TeV. Jets with transverse momenta in the range of 20 < jet p_{T} < 100 GeV/c are investigated, using several resolution parameters between R = 0.2 and R = 0.6. The published results are compared to the output of Monte Carlo event generators. In this thesis Pythia8 simulations are compared to the data. The implementation of an analysis in Rivet, allows for comparison with further generators in the future and is a way to preserve the analysis.

Zusammenfassung:

Auf Grundlage der Implementierung einer Jet Analyse [1] der ALICE Kollaboration in dem Rivet Framework, wird eine Monte Carlo Studie durchgeführt. Gegenstand dieser Analyse bilden Wirkungsquerschnitte geladener Jets, sowie deren Fragmentationsverteilungen, Multiplizitäten und Observablen, welche ein Maß für die radiale Ausdehnung von Jets bilden. Diese werden in Proton-Proton Kollisionen bei $\sqrt{s}$ =7 TeV gemessen. Es werden Jets mit Transversalimpulsen im Intervall von 20 < Jet p_{T} < 100 GeV/c untersucht. Für die Jet-Rekonstruktion werden Radiusparameter zwischen R = 0.2 und R = 0.6 verwendet. Die Ergebnisse der bereits veröffentlichten Analyse werden dem Output verschiedener Monte Carlo Event Generatoren gegenübergestellt. In dieser Arbeit werden Pythia8 Simulationen mit den Daten verglichen. Die Implementierung einer Analyse in Rivet ermöglicht den künftigen Vergleich mit weiteren Event Generatoren und stellt eine Archivierungsmethode der ursprünglichen Analyse dar.

Contents

Chapter 1

Introduction

1.1 From early fixed-target experiments to ultra-relativistic heavy-ion collisions

Since the development of the first particle accelerator in 1928 [2], more and more accelerators were built with continuously increasing centre of mass energies of the colliding particles. The first accelerators were based on electrostatic force. In 1932 the first induced nuclear disintegration was observed in an experiment which involved accelerating protons along a vacuum tube towards a Lithium target [3]. In this early fixed-target experiment the projectiles were accelerated to kinetic energies of about 400 keV. Shortly thereafter the first cyclotron was built. They were found to be much more efficient than linear accelerators, based on static fields, for the acceleration of light particles.
Collider experiments evolved in the early 1960s [2], the first one being the electron-positron (e^-e^+) collider experiment in Frascati, Italy. The only prerequisite for particles to serve as a projectile in a high-energy accelerator being that they are stable and charged [4], further e^-e^+, proton-proton (pp and $p\bar{p}$) and electron-proton colliders (e^-p or e^+p) were built subsequently.

In the mid 1970s and early 1980s, the first experiments dedicated to heavy-ion collisions were set up at Bevalac at the Lawrence Berkeley National Laboratory. Projectiles with energies of about 2 GeV per nucleon were smashed into targets of similar heavy-ions [5]. The development of heavy-ion colliders again induced a big increase in centre of mass energy. The highest energy reached so far in the centre of mass system E_{cms} for heavy-ion collisions was at the Large Hadron Collider (LHC) at CERN, the European Organization for Nuclear Research, in Switzerland and France. At the LHC collisions of lead (Pb) nuclei with atomic number 82 and mass number 208 are observed. By now E_{cms} amounts to about 574 TeV ($2 \cdot 82 \cdot 3.5$ TeV) and is soon to be almost doubled.

The collision energy has hence reached macroscopic sizes in heavy-ion collisions and is 10^6 times larger than in the first accelerator experiments about a hundred years ago. Due to this rapid increase of collision energy and the setting-up of different high energy particle experiments, tremendous progress has been made in the exploration of the physics at the smallest accessible length scales, during the past century. Several particles and phenomena that had been theoretically predicted beforehand were

detected in these experiments. Several discoveries were made, based on Standard Model predictions. Among these were the discoveries of the τ neutrino and the W and Z bosons. The most recent discovery was the finding of the Higgs boson at the LHC [6, 7] and hence all particles predicted by the Standard model have been detected experimentally.

The following section presents the particle content of the Standard Model and the fundamental forces described therein. The central topic of this thesis are jets in proton-proton collisions. To address the relevant aspects of jets, basic knowledge about the strong force is crucial, which will therefore be introduced in more detail.

1.2 The Standard Model and quantum chromodynamics

The particle content of the Standard Model of elementary particles is listed in Fig. 1.1. Described are the three generations of matter, each generation consisting of a lepton and the corresponding lepton neutrino, an up-type and a down-type quark, the four gauge bosons: photon, gluon and Z and $W^{\pm}$ bosons, as well as the Higgs boson [8]. Quarks and leptons carry spin $\frac{1}{2}$ and are therefore classified as fermions. Up-type quarks carry $\frac{2}{3}$ of positive, down-type ones $\frac{1}{3}$ of negative elementary electric charge. With an electric charge of -e, the leptons μ and τ are very similar to the electron, however, with greater masses. Neutrinos are neutral and, in contrast to the predictions of the Standard Model, were found to have masses unequal to zero. The masses, however, are so small ($O(10^{-9}$ GeV)) that they have not yet been determined. Anti-fermions respectively carry the opposite charge. The forces between the particles are described by the exchange of particles, the four gauge bosons named above. All four carry spin 1. Photons and gluons are massless, whereas Z and $W^{\pm}$ are about 100 times heavier than a proton. Only three of the four fundamental forces are described by the Standard Model: the electromagnetic, the weak and the strong force. Gravity is not integrated in the Standard Model. While it is negligible at typical experimentally accessible scales in particle physics, it is responsible for large-scale structure of the universe [4].

Quantum chromodynamics (QCD) is the theory of the strong interaction. It is a quantum field theory that is rather young compared to e.g. quantum electrodynamics (QED) which is the theory of electromagnetic interaction [10]. Whereas QED evolved in the first half of the last century, the main ideas that lead to the formulation of QCD emerged in the mid 1960s [11] and it took ten more years until its present form was attained [12, 13]. There are quite a few analogies between both theories. The corresponding forces, however, vary widely, especially in their spatial behaviour.[1]

The analogue to the photon in QED is the gluon. QCD interaction, i.e. the interaction of quarks, is mediated by the exchange of not just one, but eight different

[1] Since this section aims to give an overview about QCD rather than QED, see [14] for more information on QED.

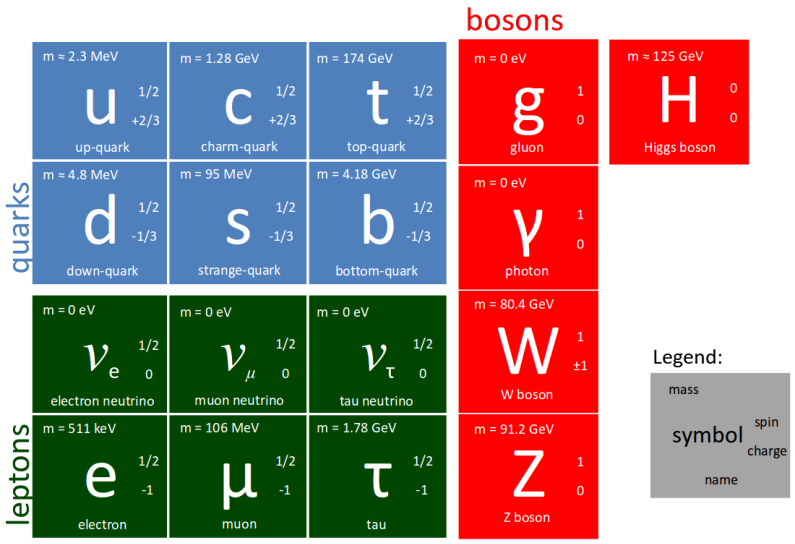

Figure 1.1: Elementary particles in the Standard Model: three generations of quarks and leptons, the four gauge bosons and the Higgs boson [9, 8]

gluons. Quarks were found to have three additional degrees of freedom which were labelled as colour charges (r, g and b). The term colour charge does not relate to physical colours. Gluons respond to colour charge similarly as a photon does to electric charge. Quarks carry one unit of positive colour charge. By convention anti-quarks carry negative colour charge or what is more commonly referred to as anti-colour. In contrast to the photon, which is neutral, the gluons do carry colour themselves. Gluon charge is a superposition of the three colours and their anti-colours. There are 9 such combinations of which only 8 are physical. This property enables them to interact with each other [10].

Coloured particles cannot be observed freely, i.e. they are confined and cannot propagate as free particles. This phenomenon is called colour confinement. It might result from the gluon-gluon self interaction. This, however, has not yet been proven analytically [4].

In QED field lines between two spatially separated charges spread out. In contrast to that, a flux tube builds up between a separated quark anti-quark ($\mathrm{q\bar{q}}$) pair. The suppression of spatial expansion might be explained by an attractive force between the gluons, mediating the force between q and $\bar{\mathrm{q}}$. The energy stored in the gluon field grows linearly with the distance r of the $\mathrm{q\bar{q}}$-pair, since the energy density is constant within the tube for relatively large distances. This is reflected in the second term of Eq. 1.1 that shows the potential between q and $\bar{\mathrm{q}}$.

$$V(r) = -\frac{4}{3}\frac{\alpha_s}{r} + kr, \tag{1.1}$$

where α_s is the coupling constant of the strong interaction and $k \simeq 1\frac{\mathrm{GeV}}{\mathrm{fm}}$ is the so-called 'string tension' [4].

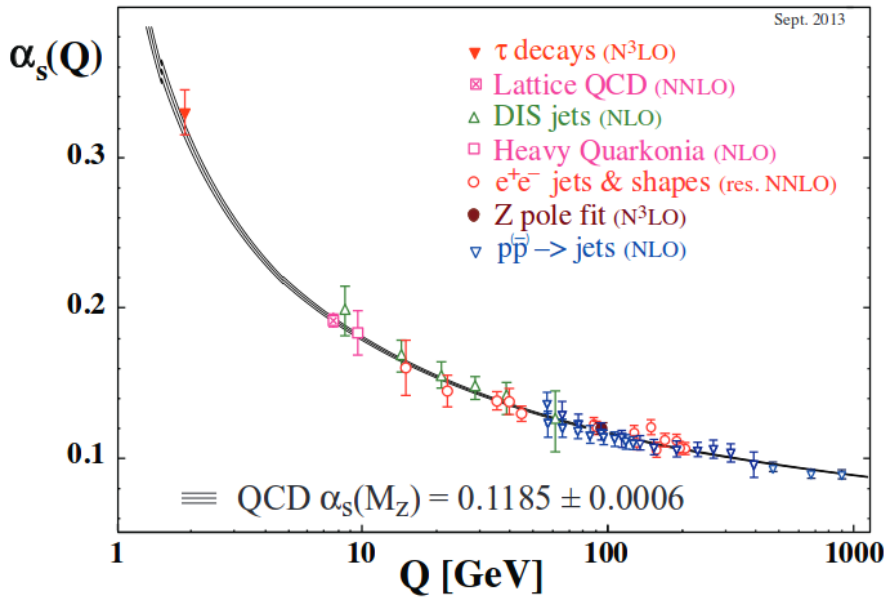

Figure 1.2: Running Coupling α_s as a function of the energy scale Q [15]

The strong coupling constant α_s is plotted in Fig. 1.2 against momentum transfer Q that can be translated into spatial distance. A high momentum transfer results in high spatial resolution, i.e. corresponds to short distances. At small momenta, i.e. large distances, the coupling constant becomes very large. The perturbation expansion in α_s does not converge and perturbative QCD breaks down in this regime. Processes involving large distances/ small momentum transfers, such as hadronisation cannot be calculated from first principles up to now and phenomenological models (see section 2.1) must be used for the description. At smaller distances (large momenta), however, α_s tends to 0. This is referred to as asymptotic freedom and in this regime quarks and gluons are coupled weakly [4, 16].

The quark-gluon plasma (QGP) is thought to be a state of QCD matter in which quarks and gluons are deconfined. The transition to such a deconfined phase requires high temperatures and/or large net-baryon densities. Critical temperatures T_c for the transition are estimated to be about 150 MeV in units of $k_B T$, corresponding to approximately $2 \cdot 10^{12}$ K [17]. This value is obtained from lattice QCD[2] calculations at zero net-baryon density. The energy density reached in current heavy-ion collisions is assumed to be sufficiently high, that these temperatures and densities are reached in the centre of a collision. A broad variety of measurements indicate the presence of QGP in those collisions [18, 19]. However, a direct proof of the existence of the QGP has not yet been delivered. Investigations on the QGP are of high interest, because they might shed light on the early stages of the universe. The universe

[2]Lattice QCD is an approach to solve the theory of quantum chromodynamics non-perturbatively on a space-time-lattice. In the case of infinite expansion of the lattice and infinitesimally small lattice spacing the QCD continuum is recovered.

is thought to have been in this state of matter about $10 \cdot 10^{-12}$ s after the Big Bang, which should have lasted for about $10 \cdot 10^{-6}$ s, prior to the hadronisation process [19]. Several experiments are designated to explore this QCD medium by observing heavy-ion collisions. At the moment three experiments at the LHC collect data from nucleus-nucleus collisions: ATLAS, CMS and ALICE. The latter is the one dedicated to heavy-ion collisions at LHC and will be dealt with in the following section.

1.3 A Large Ion Collider Experiment

'A Large Ion Collider Experiment' (ALICE) is one of the four major experiments at the LHC. The two biggest experiments CMS (Compact Muon Solenoid) and ATLAS (A Torroidal LHC ApparatuS) both use general-purpose detectors [20]. They both pursue the same scientific goal, i.e. the search for new physics, such as extra dimensions[3] and dark matter particles. If new discoveries are made, a direct cross check is ideally provided by the respective other experiment.

The LHCb experiment is focused on the study of the b (bottom or beauty) quark, as is indicated by the name of the experiment. LHCb studies the differences of matter and anti-matter. ATLAS, CMS and LHCb primarily investigate proton-proton (pp) collisions of up to 14 TeV centre of mass energy [20].

ALICE is optimized to study heavy-ion collisions in order to search for and gain knowledge about the QGP. As a reference for lead-lead (Pb-Pb) collisions, but also for supplementary studies to the ones conducted by the other three experiments, proton-lead (p-Pb) and pp collisions are studied as well. The lead nuclei are collided at a design centre of mass energy of up to $\sqrt{s_{\mathrm{NN}}} = 5.5$ TeV per nucleus-nucleus pair. The event multiplicities of heavy-ion collisions at such energies are extremely high: about 3000 charged particles per event. ALICE is optimized to cope with such extremely high charged particle multiplicities.

In Fig. 1.3 the set-up of the ALICE detector is shown. The individual detectors are mentioned in the order that reflects the distance to the interaction point, starting with the closest one.

The beam pipe is surrounded by the six-layers of silicon detectors of the Inner Tracking System (ITS). The ITS is used for tracking and high precision determination of decay vertices [18]. The Time Projection Chamber (TPC) is the most important tracking device in ALICE and the largest detector of its kind ever built. The TPC is contained within the 18 segments of the Transition Radiation Detector (TRD). Besides providing additional track information the TRD is used for triggering and identification of electrons. It is surrounded by the Time-Of-Flight detector (TOF). The measurement of the transit time of flight at intermediate momenta which can be translated into particle velocity serves particle identification (PID) purposes. On the outer surface of TOF, two electromagnetic calorimeters, EMCal and PHOton

[3] This might explain why the gravitational force is so weak compared to the other fundamental forces.

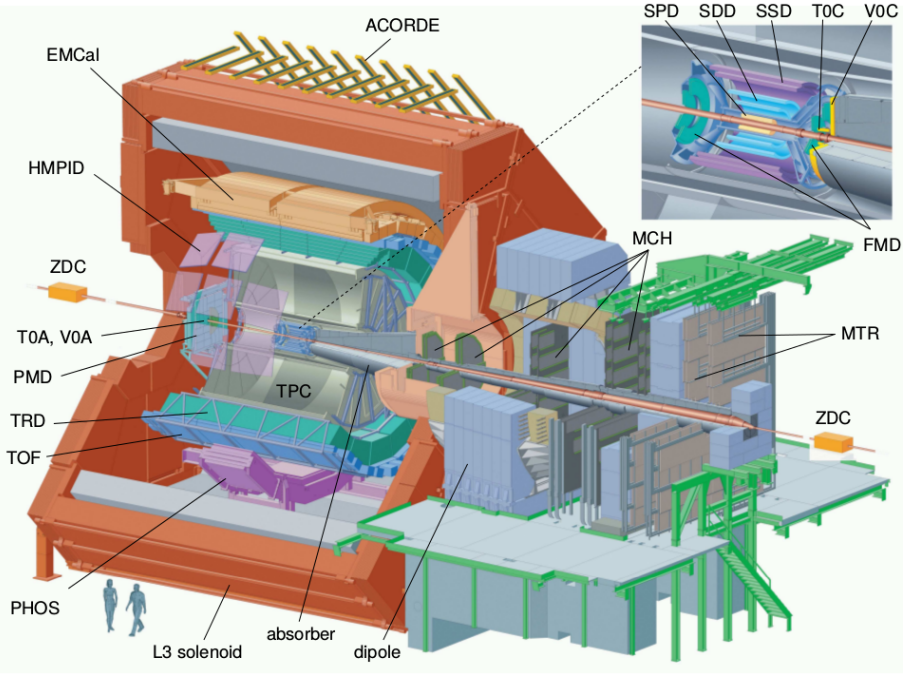

Figure 1.3: Set-up of ALICE showing the sub-detectors as well as the muon arm [21]

Spectrometer (PHOS) and a Ring Imaging Cherenkov detector, HMPID, are installed that respectively do not cover the full azimuthal angle. The purpose of the HMPID is reflected by its name which stands for High Momentum Particle Identification Detector.

The detectors mentioned above can be summarized as central barrel detectors [21]. Additional smaller detectors, placed in forward direction, are used for triggering and event characterisation. The detectors with this purpose are the Photon Multiplier Detector (PMD), the Zero Degree Calorimeter (ZDC) and the three Forward Detectors (FWD): V0, T0 and the Forward Multiplicity Detector (FMD). The central barrel is contained within a solenoidal magnet that generates a magnetic field of about 0.5 Tesla. One side of the ALICE detector is supplemented by a muon arm, used for measurements of charmonium and light vector meson production and detection of high p_{T}-muons. The magnetic field of the muon arm is generated by a dipole magnet ($\int B \, \mathrm{d}l = 3.0$ Tm).

The analysis presented in this bachelor thesis is exclusively based on Monte Carlo event generated data on particle level, i.e. detector effects are not taken into account. The individual components of the ALICE detector will therefore not be explained in more detail. See the ALICE performance papers for more information on the individual detectors [21, 22].

1.4 Outline

This thesis is organized as follows. Chapter 2 introduces the relevant aspects of jet physics. In this chapter also a detailed description of jet reconstruction algorithms is given and the jet observables that are evaluated in this thesis are defined and discussed. In chapter 3 Monte Carlo event generators used for the simulation of pp collisions are introduced. The generation process of the Pythia event generator is described. Chapter 4 gives an overview about the functions and the use of the analysis tool-kit Rivet. General information and a description of the corrections applied to the corresponding as well as the Rivet analysis can be found in chapter 5. Results of the Rivet analysis are presented and discussed in chapter 6. Chapter 7 summarizes the results of this work and provides a brief outlook.

Chapter 2

Jet physics

Due to the confinement phenomenon, coloured quarks and gluons cannot be observed freely. Hadrons consist of two or three[1] coloured quarks that are composed in a way, that the hadron itself is colourless. In particle collisions quarks and gluons can be produced in the hard scattering of the incoming partons, i.e. quarks and gluons within the incoming hadrons. The fragmentation of the outgoing quarks or gluons[2], carrying high transverse momenta (p_{T}), leads to collimated sprays of hadrons – jets. Observing jets is therefore the closest one can get to 'seeing' quarks and gluons. The terms parton and jet are sometimes even used synonymously in literature, if it is assumed that each outgoing parton fragments into a jet and that the measured jet four-momentum reflects the initial parton four-momentum [23]. The strong correlation between jets and the partons becomes clear if one looks at how jets are produced in hadron collisions.

2.1 Jet production

The process of fragmentation can be understood by a simple colour string breaking model [24]. This model applies for jets in hadron-hadron collisions, as well as for jets from electro-weak production. In the latter, however, the outgoing partons result from conversion of gauge bosons into a quark-antiquark pair.

The potential between a quark-antiquark pair grows linearly for distances larger than $d \approx 1$ fm (see Eq. 1.1). For a given distance the 'colour string' breaks, as it is energetically favourable that a new quark-antiquark pair is created in between. Now there are two $\mathrm{q\bar{q}}$ pairs that respectively can undergo the same process again, given the invariant mass of the subsystems is sufficiently large and the $\mathrm{q\bar{q}}$ distance exceeds the limit again.

Two quarks created in hard scattering processes in pp collisions usually carry high transverse momenta p_{T}. Therefore 'string breaking' may take place several times until the quarks are finally bound in colourless hadrons. Two final state quarks are expected to be observed as two jets that show a back-to-back correlation. Due to

[1] By now particles compatible with pentaquarks – exotic hadrons that consist of more than three quarks – have been observed [20]

[2] in the following referred to as outgoing partons, although originally the term parton only described the constituents – the parts of hadrons

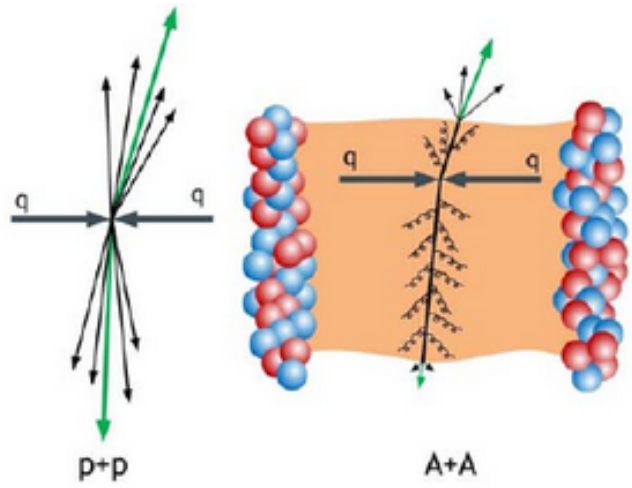

Figure 2.1: Comparison of jets in pp and A-A collisions [27].

acceptance limitations of the detectors, often only one jet per event is observed. In the case that an event contains more than one jet, the one with the highest p_{T} is referred to as the *leading jet*.

2.2 Jets in heavy-ion collisions

As mentioned in section 1.2, a hot and dense medium forms, when heavy ions collide at ultra-relativistic energies. The formation of the medium and the evolution of jets take place on larger time scales than the hard scattering of the partons. Highly energetic partons traversing the medium can lose energy via medium induced gluon radiation and elastic scattering. The energy loss of these partons results in less energetic jets. Jets corresponding to the same parton energy in pp collisions, will on average have a reduced energy in Pb-Pb collisions. This process is referred to as jet quenching. It had been first proposed by Bjorken in 1982 [25] and was observed experimentally about 18 years later at RHIC [26].

At the energy scales that are reached so far, the possible formation of the QGP is restricted to A-A collisions only. By comparing jets in pp and p-A collisions to jets in A-A collisions, conclusions may be drawn about the parton-medium interaction. In addition to the reduction of jet energy, several jet observables should be modified, if further interactions between the partons and the medium have taken place. The measurement of jet properties is therefore a strong indicator whether the medium has formed or not. Figure 2.1 illustrates the phenomenon of jet quenching in the presence of the medium in heavy-ion collisions.

2.3 Jet reconstruction

2.3.1 Jet reconstruction algorithms

In order to find the particles that could be constituents of a certain jet, jet reconstruction algorithms are used in high energy physics analyses. This is a rather difficult task and the algorithms need to be well defined to allow theory comparisons. There are two widely used classes of jet finding algorithms: cone-type and sequential recombination algorithms. For both types the user defined radius parameter R determines the angular reach of the jet reconstruction. Typical values of R range from 0.2 to 1.

Cone-type algorithms are based on the iterative search for so called "stable cones" in the $\eta - \varphi$ plane. The idea that brought about those algorithms is to picture jets as angular cones around some direction of dominant energy flow [28]. In order to find those directions, various particles are taken as seeds, i.e. initial guesses for the cone axis. For each seed, all particles in a cone within a certain radius parameter R are clustered. The resulting 4-momentum is then used as a new direction for the cone. The iteration terminates when a stable, non "flowing" cone is reached, i.e. the cone axis does no longer change.

Sequential recombination algorithms repeatedly combine pairs of particles (pseudojets) to pseudojets (jets). They introduce a distance measure between two entities (particles and pseudojets):

$$d_{ij} = min(k_{\mathrm{T}i}^{2p}, k_{\mathrm{T}j}^{2p}) \cdot \frac{\Delta_{ij}^2}{R^2} \qquad\qquad d_{iB} = k_{\mathrm{T}i}^{2p}, \tag{2.1}$$

where $\Delta_{ij}^2 = (y_i - y_j)^2 + (\varphi_i - \varphi_j)^2$ and the variables $k_{\mathrm{T}i}, y_i$ and φ_i are respectively the transverse momentum, rapidity and azimuthal angle of entity i [29]. The p in the exponent determines the type of algorithm. For the k_{T} algorithm, the value $p = 1$ is taken, for the Cambridge/Aachen algorithm $p = 0$ and for the anti-k_{T} algorithm $p = -1$ [29]. Entities that are closest to each other are recombined until there are no entities left that fulfil the distance criterion. In the following criterion d_{ij} is introduced as the distance between two entities and d_{iB} as the distance between entity i and the beam B.
If d_{ij} is smaller than d_{iB}, entities i and j are recombined. If the entity-beam distance is smallest, entity i is listed as a jet and removed from the list of entities.

A common choice for jet reconstruction in pp and heavy-ion collisions at the LHC is the anti-k_{T} algorithm [29]. The reason for that is illustrated in Fig. 2.2, showing a sample parton-level event. To characterise jet areas, random soft "ghost" ($p_{\mathrm{T}}^{ghost} \to 0$) particles were added to the list of particles of the event. It is illustrated which ghosts are clustered into the different jets, which defines the jet area. For the anti-k_{T} algorithm the jet areas are much more circular than e.g. for the k_{T} algorithm case. Low p_{T}, i.e. soft particles, do not strongly influence the jet area shape, since the exponent for the anti-k_{T} algorithm is negative in Eq. 2.1. This feature is very important for hadron-hadron collisions due to the contribution of underlying event

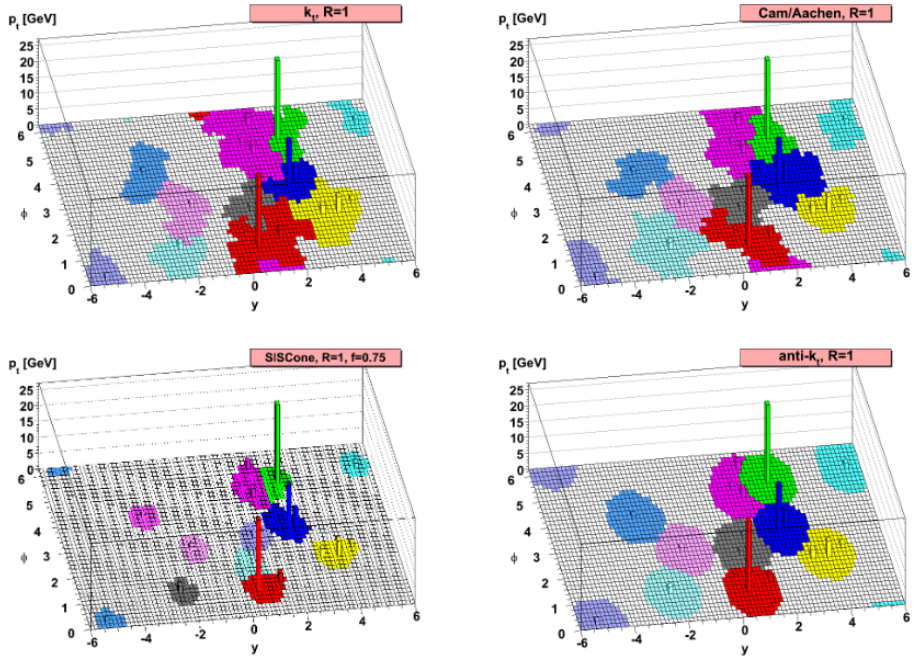

Figure 2.2: Comparison of the jet area for the same parton-level event, together with random soft "ghosts", reconstructed with the four clustering algorithms k_{T}, anti-k_{T}, Cambridge/Aachen and SISCone [29]

(UE) and high pile-up in pp collisions at the LHC. The UE can be classified as mostly low-p_{T} particles that are neither constituents of jets nor result directly from the hard scattering processes. Pile-up relates to particles produced in multiple pp interactions that also occur within the sensitive time of the detector, not related to the primary pp interaction. These additional interactions also result in mostly soft particles that contribute to the measured observables. By the use of anti-k_{T} the influence of UE and pile-up on the jet shape is minimised.

2.3.2 Reconstruction of charged jets in ALICE

Calorimeters are often used for the reconstruction of jets due to their good energy resolution at high energies [30]. ALICE is optimized for rather low p_{T} jets (< 100 GeV/c), since they are most relevant in heavy-ion collisions. Jet reconstruction in ALICE is therefore mostly based on tracking, yet combined with electromagnetic calorimeters (EMCal and DCal). They, however, do not cover the full azimuthal angle.
Some analyses are based on the reconstruction of full jets and some on jets, only reconstructed from charged particles. For full jets, both the tracks of the charged particles and the information of the calorimeters are used for reconstruction [21]. In [1] only charged tracks, that are reconstructed in the central barrel (in the TPC and ITS) are used for the jet reconstruction. This allows for jet reconstruction over the full azimuthal angle.

The η acceptance of the ALICE detector for tracking is $|\eta| < 0.9$. Only tracks with $p_{\mathrm{T}} > 150$ MeV/c are accepted. The fiducial jet acceptance for jets, reconstructed with radius parameter R, is $|\eta^{\mathrm{jet}}| < (0.9 - R)$ to warrant full overlap. In this work the FastJet anti-k_{T} algorithm [29], based on a boost invariant p_{T} recombination scheme, is used. No particle identification is used for jet reconstruction in ALICE and the particle masses are therefore set to zero.

2.4 Jet observables

There is a variety of observables that characterise jet properties. This section introduces the jet observables presented in this thesis, i.e. their definition and methods how they are measured. This includes the inclusive differential jet cross section, the charged particle multiplicity in leading jets $\langle N_{ch} \rangle$, the leading jet size $\langle R_{80} \rangle$, the radial distribution of p_{T} within the leading jet $\langle \mathrm{d}p_{\mathrm{T}}^{sum}/\mathrm{d}r \rangle$, and jet fragmentation distributions $F^{p_{\mathrm{T}}}$, F^{z}, F^{ξ}. This set of jet observables follows the one presented in [1]. The analysis presented in this work is constrained to charged jets, as will be explained in section 2.3.2.

Jet cross sections show the frequency distribution of jets with certain transverse momenta accumulated in many events. The following relation shows how the differential charged jet cross section is evaluated:

$$\frac{\mathrm{d}^2\sigma^{\mathrm{jet},ch}}{\mathrm{d}p_{\mathrm{T}}\mathrm{d}\eta}(p_{\mathrm{T}}^{\mathrm{jet},ch}) = \frac{1}{\mathcal{L}^{int}} \frac{\Delta N_{\mathrm{jets}}}{\Delta p_{\mathrm{T}} \Delta \eta}(p_{\mathrm{T}}^{\mathrm{jet},ch}), \tag{2.2}$$

where $\mathcal{L}^{int}$ is the integrated luminosity ($\mathcal{L}^{int} = \int \frac{1}{\sigma} \frac{\mathrm{d}N}{\mathrm{d}t} \mathrm{d}t$) and ΔN_{jets} is the number of jets in the selected intervals of Δp_{T} and $\Delta\eta$.

The charged particle multiplicity in leading jets, N_{ch}, is defined as the number of constituents of the leading jet. The computation of the mean charged particle multiplicity $\langle N_{ch} \rangle$ in bins of jet p_{T} indicates the correlation between $\langle N_{ch} \rangle$ and the p_{T} of final state partons.

One way to measure the spatial extent of the leading jet is by calculating R_{80}. It is defined as the radius in the $\eta - \varphi$ plane containing 80% of the total p_{T} found in the jet cone [1].

The distribution of p_{T} density, $\mathrm{d}p_{\mathrm{T}}^{sum}/\mathrm{d}r$, within a leading jet gives an insight on how the transverse momenta of the jet constituents are distributed within a jet. It therefore also provides information about the spatial extent of jets. It is measured as a function of the distance $r = \sqrt{(\Delta\eta)^2 + (\Delta\varphi)^2}$ from the jet direction. The momentum density is calculated jet by jet as a scalar sum of the transverse momenta, p_{T}^{sum}, of all charged particles produced in concentric regions of width Δr at radius r, the centre of these regions being the jet axis. Figure 2.3 illustrates the measurement of the distribution of p_{T} density. The mean value of the momentum density, $\langle \mathrm{d}p_{\mathrm{T}}^{sum}/\mathrm{d}r \rangle$, is evaluated as a function of r using the following relation:

$$\langle \frac{\mathrm{d}p_{\mathrm{T}}^{sum}}{\mathrm{d}r} \rangle (r) = \frac{1}{\Delta r} \frac{1}{N_{\mathrm{jets}}} \sum_{\mathrm{i}=1}^{N_{\mathrm{jets}}} p_{\mathrm{T}}^{\mathrm{i}}(r - \Delta r/2, r + \Delta r/2), \tag{2.3}$$

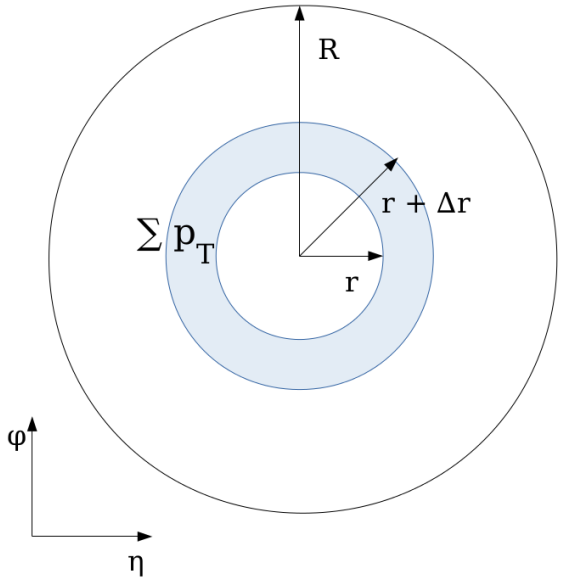

Figure 2.3: Illustration of the p_{T} density measurement

where $p_{\mathrm{T}}^{\mathrm{i}}(r - \Delta r/2, r + \Delta r/2)$ denotes the summed p_{T} of all tracks of jet i, inside the annular ring between $r - \Delta r/2$ and $r + \Delta r/2$. The mean value is reported in bins of jet p_{T}, N_{jets} denoting the number of jets per bin [1].

Fragmentation distributions give an insight on how the transverse momenta ($p_{\mathrm{T}}^{particle}$) are distributed among the particles within a jet. In order to also emphasize fragmentation into constituents with low p_{T} the variable $\xi^{ch} = \log(1/z^{ch})$ is introduced, where z^{ch} equals $z^{ch} = p_{\mathrm{T}}^{particle}/p_{\mathrm{T}}^{jet,ch}$. In this work the fragmentation of leading jets is presented based on the following distributions:

$$F^{p_{\mathrm{T}}}(p_{\mathrm{T}}, p_{\mathrm{T}}^{jet,ch}) = \frac{1}{N_{jets}} \frac{\mathrm{d}N}{\mathrm{d}p_{\mathrm{T}}}, \tag{2.4}$$

$$F^{z}(z^{ch}, p_{\mathrm{T}}^{jet,ch}) = \frac{1}{N_{jets}} \frac{\mathrm{d}N}{\mathrm{d}z^{ch}}, \tag{2.5}$$

$$F^{\xi}(\xi^{ch}, p_{\mathrm{T}}^{jet,ch}) = \frac{1}{N_{jets}} \frac{\mathrm{d}N}{\mathrm{d}\xi^{ch}}, \tag{2.6}$$

where N is the number of charged particles. Due to the fact that only charged particles are taken into account, $p_{\mathrm{T}}^{jet,ch}$ does not include the p_{T} carried by neutral particles.

Chapter 3

Monte Carlo event generators for the simulation of pp collisions

Physics aims to put forward a better understanding of nature. On the one hand theoreticians make assumptions and predictions and try develop a theory. On the other hand, experimentalists observe physical quantities by making experiments. But both experimentalists and theoreticians depend on each other's confirmation.

In particle physics, theory and phenomenological models are implemented in Monte Carlo event generators (MC generators). Full simulations of collision events[1] are performed with such MC generators and the output can be weighed against experimental data. They are therefore a powerful interface between experiment and theory of particle phyiscs.

Monte Carlo methods are not only relevant for the simulation of HEP processes, but are widely used for all kinds of scientific problems that cannot be solved analytically. Monte Carlo simulations are based on the use of random numbers and probability distributions. By simple hit-or-miss techniques, analytically unsolvable integrals can be calculated using MC methods.

For simulation of physics processes the way MC methods are applied differ. Take for example a simplified physical system with only two possibilities of how it will behave. They are assigned with the two probabilities p1 and p2 = 1 - p1. A random number between 0 and 1 is generated and, depending on the value (larger or smaller than p1), the system behaves accordingly.

For the simulation of high-energy particle collisions several MC methods are combined. Both the probabilistic approach and the evaluation of integrals are used.

3.1 General purpose event generators

The main goal of general purpose Monte Carlo event generators (GPMC) is full simulation of collision events. They provide an interface for the application of more specialized tools for specific sub-processes and are therefore used for various purposes. GPMCs such as Pythia [31], Herwig [32] and Sherpa [33] are most commonly used

[1] A generated event is basically a list of particles, often containing more information on particle properties than real data.

for simulations of pp events. In general, despite some extensions, they do not address collisions involving nuclei with mass numbers $A \geq 2$ [34]. The general approach is to start from perturbative QCD (pQCD) and use perturbative expansion, mostly leading order (LO), for the hardest interaction between two partons. This is combined with non-perturbative detailed models of hadronisation and multiparton interactions (MPI).

The simulation process is described in the following section with a special focus on the Pythia generator[2] which is used for the event generation in this thesis. The main ideas hold for all general purpose event generators, implemented models, however, differ.

3.2 Simulation process

Owing to its complexity the generation process is subdivided in different parts. At first two incoming beams are directed towards each other. For hadron collisions the partonic substructure of the incoming particles is described by parton distribution functions (PDF)[3]. The main characteristics of an event are defined by the hard process, the interaction of two partons with high momentum transfer. Independently of whether the hard process has yet taken place, quarks and gluons may branch and initiate parton showers. The underlying event is simulated based on models, e.g. multiple parton interaction (MPI). In the hadronisation step, coloured partons are transformed into colourless hadrons. The final step is to simulate further decay of unstable final state particles [31].

3.2.1 Hard process

Simulations usually begin with the calculation of the hard process which defines the main characteristics of a collision event. The hard process involves high 4-momentum transfers Q^2. At these scales α_s is sufficiently large so that the hard process can be evaluated perturbatively. A variety of hard processes are implemented in MC generators. They are distinguished by the number of particles in the final state. A typical $2 \rightarrow 2$ process would be a highly energetic collision of two incoming partons resulting in two outgoing final state partons. The relevant production cross sections can be calculated from the PDFs, the differential parton-level cross sections for the production of certain final states, through the initial partons, and integration over the corresponding phase space over the final-state particles (see e.g. Eq. (1) in [35]).

Most generators treat the hard process at leading order of perturbation theory, i.e. at the lowest relevant order. In order to make predictions that are more precise, higher orders may also be taken into account. The implementation of the hard process is relatively uniform within GPMCs, despite the fact that the PDFs differ

[2] Pythia6 is the original Pythia generator written in Fortran, and Pythia8 is a rewrite in C++.

[3] PDFs are defined as the probability density for finding a parton with a certain longitudinal momentum fraction x of the total proton momentum for a certain Q^2 [4]

for generators and tunes [35, 31]. PDFs cannot yet be derived from first principles. Nevertheless the parton evolution functions (DGLAP) can be used to calculate their Q^2 dependence and further information can be extracted from measurements [4].

Pythia is optimized for $2 \rightarrow 1$ and $2 \rightarrow 2$ processes [31]. The current default PDF set is CTEQ 5L and only leading order calculations are performed [36], if not explicitly induced otherwise.

3.2.2 Parton showers

The behaviour of the coloured partons is described by the parton shower phase of an event generator. Incoming initial- and final state partons may start of a sequence of branching. The equivalent to photon radiation in QED, when charged particles are accelerated, is gluon radiation in QCD. High p_T quarks can radiate off gluons $q \rightarrow qg$ and thereby lose energy. Since gluons carry colour charge themselves, gluons can emit gluon radiation as well. Furthermore, gluons may convert into a quark anti-quark pair and the quarks, if sufficiently energetic, may branch as well. All these processes lead to a cascade of partons – parton showers. Depending on whether the hard process has yet taken place, they are classified as initial- and final-state parton showers.

Parton shower algorithms are typically formulated as an evolution in some chosen scaling variable which is often associated with the mass m^2 or transverse momentum ${p_T}^2$ of the branching parton. Starting at high scales associated with the hard process, a parton is evolved in this variable down to low scales of about 1 GeV. At this scale, the showering algorithm terminates and non-perturbative confinement effects set in [35, 31].

Parton showering in Pythia8 and recent versions of Pythia6 is based on p_T-ordering [31, 36].

3.2.3 Hadronisation

When the energy of the partons has fallen below a certain threshold, hadronisation sets in. The hadronisation process cannot be described by perturbative QCD, due to the fact that perturbation theory breaks down, as α_s becomes large. This lead to the development of different phenomenological models, of how the coloured partons are transformed into colourless hadrons. The term hadronisation is often used to describe both fragmentation, the transformation into colour singlet states, and further decay of unstable final state particles. The three main fragmentation models, implemented in event generators are string fragmentation, independent fragmentation and cluster fragmentation [31]. In Pythia the Lund String model is used, which is sketched in section 2.1.

The simulation of the decay of unstable final state particles into stable hadrons, leptons and photons, requires an exact implementation of particle properties and decay channels. This simulation step might appear straight forward, but is strongly impeded by the lack of knowledge about several decay properties and the complexity

of certain decays. Pythia makes use of several tables that include decay modes and branching ratios. These tables can be modified by the user to study or modify certain decay channels [31].

3.2.4 Underlying event

Different models exit, describing the dynamics of the hadron remnants that are not involved in the hard process. However, only multiple parton interactions are introduced here, since this is the model implemented in Pythia.

The incoming protons are complex bound states of several strongly-interacting partons. This allows for the possibility of not just one parton-parton interaction, but multiple parton interactions. To calculate further, softer interactions, the PDFs are modified to account for the reduced number of partons in the beam remnant. Primarily soft partons are created, but also hard and semi-hard partons can be produced albeit with small probabilities. They undergo the same processes as the ones from the hard-process and can contribute to all observables [35].

3.3 Generator tunes

The goal of complete agreement between generator output and real data will not be met until the entire underlying physics of HEP processes is fully understood and can be calculated from first principles. As becomes clear in the previous section, we are currently very far away from that. Therefore there are several models and parameters, that are weakly constrained from theory and experiment, implemented in MC generators. These 'degrees of freedom' give rise to a number of different tunes of certain generators. The number of changeable parameters vary for the different generators. Possible changes in Pythia can be made for example in the set of PDFs, fragmentation and parton shower cut-off scales and values of the strong coupling constant α_s for different stages in the simulation [31]. The ultimate goal of generator tuning is the finding of sets of parameters, so that the generator output agrees as accurate as possible with data.

The two tunes that are used in this thesis both take into account LHC data and are standard tunes for comparison to LHC results. The current default tune of Pythia8 for pp simulation is tune 4C. It was developed shortly after first results of LHC Run 1 had been evaluated. Tune 4C proved to agree with LHC data slightly better than previous tunes and became default [37].

MONASH 2013 was developed after Run 1 and therefore more LHC data, together with data from Tevatron and SPS, had been taken into account. The goal was to re-optimize final-state radiation and hadronisation parameters, as well as to try out new sets of PDFs. A list of all parameters comparing MONASH 13 to tune 4C can be found in [38]. In table 3.1 a small selection of changed tuning parameters is listed. The two tunes use different PDFs to describe the substructure of the incoming protons. Changes in the hard process α_s, which is used to calculate the cross sections,

were shown to directly affect low-p_{T} regions as well as jet cross sections at high p_{T} in [39]. The MPI α_{s} value is used for the calculation of MPI cross sections and allows to control the UE activity. It is usually set to the same value as the hard process α_{s}. A more detailed discussion of the different parameters, goes beyond the introductory purpose of this section. Please see [38] for a detailed comparison between both tunes.

Table 3.1: Set of Pythia8 tuning parameters of the Monash 2013 and 4C tune [38]

Parameter	**MONASH 13**	**Tune4C**	**Comment**
PDF set	NNPDF2.3 QCD+QED LO	CTEQ6L1 LO	PDF set for the proton
Hard process α_{s}	0.130	0.135	α_{s} for cross section calculation
MPI α_{s}	0.130	0.135	α_{s} for MPI

Chapter 4

Rivet framework

The objective of this work is the implementation of an analysis performed by the ALICE Collaboration in Rivet. The main goal of such a Rivet analysis is to preserve the analysis algorithm that had previously been applied to experimental data. It is therefore very important, that the Rivet analysis code accurately reflects the original analysis code. The Rivet analysis, presented in this thesis, corresponds to the measurement of charged jet cross sections and properties in pp-collisions at $\sqrt{s}$ =7 TeV using the ALICE detector at the LHC, published in Oct 2014 [1].

Rivet [40] stands for *Robust Independent Validation of Experiment and Theory*. It is a C++ framework which is used to perform high-energy physics (HEP) analyses exclusively for Monte Carlo studies and their comparison to experimental measurements. The input to Rivet are simulated collision events that must be provided in HepMC[1] [41] format, i.e. event generator data is stored in a certain generator independent way. A Rivet analysis therefore does not depend on the generator type. This allows for a proper comparison between different event generators. Hence one major application of Rivet is, that it can be used for the tuning of MC event generators. But since this application of Rivet is not central for this thesis, it will not be discussed in more detail.

4.1 Technicalities of Rivet

The Rivet work-flow is divided in three parts: simulation, analysis and comparison. It is shown schematically in Fig. 4.1.

A variety of different MC event generators can be used to simulate events. This is done prior to the Rivet run. The only prerequisite is, that the output has to be stored in the HepMC format. Generators written in C++ such as Pythia8 [36], Sherpa [33] or Herwig++ [42] can directly produce output in the required format. For other generators however, e.g. those written in Fortran, such as Pythia6 [31], this is not the case. AGILe [43] "A Generator Interface Library and executable" has to be used, that allows to save the output of such generators in HepMC format.

HepMC files can become very large, about 2 MB per 10 events. Hence it is common practice not to store the .hepmc files, but to use file-system pipes that work on the

[1] "An object oriented event record written in C++ for HEP MC generators"

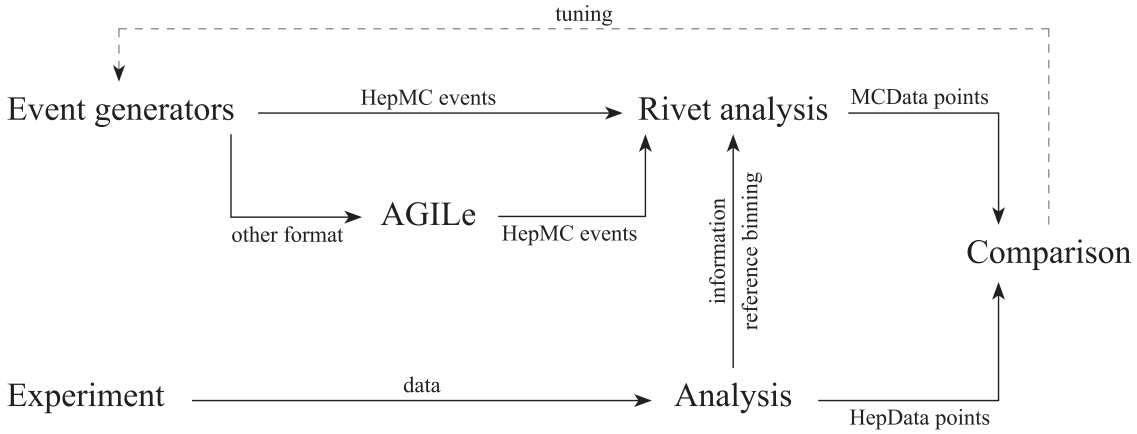

Figure 4.1: Work-flow of the Rivet analysis tool-kit

first-in, first-out principle (FIFO). Instead of reading the events from a file, Rivet reads from a text stream. Every generated event is analysed directly, and deleted afterwards.

The histogramming of Rivet is handled via the YODA[2] package [44]. After the analysis is finished a Rivet.yoda file is created by default and can be used to create histograms. The YODA package provides different histogram types: standard histograms, profile histograms that display the mean value of y for each bin in x and scatter plots which are just a collection of one, two or three dimensional data points with errors which are used to store e.g. ratios of two histograms. YODA provides a tool that allows to combine the statistics of several independent runs. This tool, however, is not yet capable of merging scatter plots since too little information is provided.

If the internal plotting options of Rivet are used, plots are created containing both reference and MC data. The flexibility of this plotting method, however, is limited. In order to be able to work with those histograms in ROOT the yoda2root script may be used.

In the case that Rivet code is not only written for own comparison purposes, but is supposed to be published with Rivet, some general guidelines, regarding the coding style, should be followed. Rivet has a certain naming convention for the analyses:
"The first part is the experiment name, the second is the year of publication, and the third is the ID code for the corresponding paper in the Inspire HEP database, preceded by an "I"." [45]
The name of this Rivet analysis is therefore ALICE_2014_I1328629.

After a validation procedure, the code will be implemented in the next Rivet release as a built-in analysis[3]. Each built-in analysis contains four analysis files: a .cc file,

[2]YODA (*Yet more Objects for Data Analysis*) is a "small set of data analysis (specifically histogramming) classes".

[3]The Rivet version used for this analysis, Rivet2.2.1, contains 313 built-in analyses of which only 6 are ALICE analyses.

containing the analysis code, a .yoda file with the reference HepData points, a .plot file with plotting information and an .info file containing general information about the analysis. The MC comparison to experimental data of published Rivet analyses, can be found on the CERN MCplots web-page [46, 47].

Rivet is currently only supported for Unix/Linux systems. To remain a relatively small package, Rivet depends on a variety of other installations that are handled individually. See the Rivet manual for further information [40]. The version that is used for this analysis is Rivet2.2.1, together with YODA1.3.1.

4.2 The structure of a Rivet analysis

Within Rivet a plug-in system is used for the analyses. Analyses are classes that inherit from `Rivet::Analysis`. An object of this analysis class is instantiated during the execution of the main program.
Rivet uses so called "projections" that are basically observable calculators. They all inherit from the `Projection` base class. Events are treated as objects. Projections 'project' out physical observables of a given event. The running of a Rivet analysis is divided in the three steps `init(), analyze()` and `finalize()`.

In the initialisation process the event loop set-up is done. The projections must be added via `addProjection`. The most common projections are `FinalState` and `ChargedFinalState`. Cuts, relevant for all final state particles, should be specified here, related to these projections. Other kinematic cuts are applied during the event by event analysis. The 'booking' of profiles and histograms with the correct binning, consistently with the experimental analysis, is also done in the `init` process.

Projections are applied to the current event during the `analyze` section via `applyProjection`. Particles are selected and filtered according to the applied criteria and finally the histograms are filled.

After every single event has been analysed the `finalize` method is called. This is where histograms are scaled and normalised. Furthermore it is possible to calculate new observables, e.g. the ratio of two histograms [40, 45].

Chapter 5

Rivet analysis

This chapter summarizes all relevant pieces of information concerning this particular Rivet analysis and the corresponding ALICE publication. This includes some general information on the corresponding analysis, see section 5.1, the technique how the UE is estimated and subtracted, section 5.2, and the generation process of the MC events, section 5.3.

5.1 General information concerning the original jet analysis

The corresponding analysis [1] is based on data collected during LHC Run 1 in 2010 with the ALICE detector. The measured jet observables are presented in section 2.4. They were measured in pp collisions at a centre of mass energy $\sqrt{s} = 7$ TeV. The analysis is restricted to charged jets. The kinematic cuts applied for measurements in ALICE can be found in section 2.3.2. Jets were reconstructed with radius parameters R = 0.2, 0.3, 0.4 and 0.6. Results were obtained for jets in the transverse momentum range between $20 < p_{\mathrm{T}}^{\mathrm{jet,ch}} < 100$ GeV/c.

A comparison of three different jet finding algorithms (k_{T}, anti-k_{T} and SISCone, see section 2.3.1) showed only small deviations in the measured cross sections. The other measurements were therefore solely performed with the anti-k_{T} algorithm.

There are two levels on which jet finding algorithms applied to MC generated data can reconstruct jets: on *particle* or *detector level*. That means that the reconstruction is either based on properties of particles that are the direct output of MC event generators or properties of particles that were processed through a detector simulation[1]. Since the reference data were corrected for instrumental effects, the comparison with simulation is done at particle level only.

The results for the charged jet cross sections and properties (except R_{80}) were presented with the subtraction of underlying event (UE). Most of the results (all but the inclusive differential cross sections for R=0.2 and R=0.3) were also presented without the UE subtraction [1]. The UE correction is the only correction applied to MC generated data and is implemented in the Rivet code. The methods used to estimate the underlying event yield will be explained in the following section.

[1] GEANT is used for the ALICE detector simulation.

5.2 Correction for underlying event contribution

The UE correction is motivated by the fact that the measurements presented in the corresponding analysis serve as a reference for p-Pb and Pb-Pb. While UE contribution to the respective observables in pp is usually of the order of a few percent only, orders of up to 50% are reached in Pb-Pb.

In this work, analogous to the corresponding paper, the UE particle yield is estimated via the *perpendicular cone* approach. For each event the particle yield is measured in two circular regions, perpendicular to the leading jet cone. The radii of these circles equal the radius parameter used for the jet reconstruction. The perpendicular cones are placed at the same pseudorapidity as the jet η_{jet}, but rotated in the azimuthal angle by $\Delta\varphi = \pm\pi/2$. The UE is measured in the transverse region to avoid adding particles from another jet, directing in the opposite direction than the leading jet, to the UE. The yield of UE particles collected in these cones is assumed to be statistically equal to those in the jet cone.

The subtraction methods differ for the different observables. The abbreviation *corr* stands for corrected, *rec* for reconstructed, i.e. no corrections for UE have been applied and *perp* indicates that a variable has been measured in the perpendicular cones. The UE is subtracted on a jet-by-jet basis for the cross sections. The $p_{\mathrm{T}}^{\mathrm{jet,ch}}$ is reduced by the average p_{T} sum accumulated in the two perpendicular cones.

$$p_{\mathrm{T}}^{\mathrm{jet,corr}} = p_{\mathrm{T}}^{\mathrm{jet,rec}} - p_{\mathrm{T}}^{\mathrm{sum,perp}}. \tag{5.1}$$

After this correction has been applied, equation 2.2 is used to calculate the corrected cross section.

For the constituent multiplicities, the distributions of p_{T} density and the fragmentation distributions, the reconstructed jet energy is not corrected for UE contamination, i.e. $p_{\mathrm{T}}^{\mathrm{jet,rec}}$ is used to calculate the observables, depending on $p_{\mathrm{T}}^{\mathrm{jet,ch}}$. For these observables the UE contribution to the observed distributions in each bin of $p_{\mathrm{T}}^{\mathrm{jet,ch}}$ is subtracted. The p_{T} spectra of particles in the perpendicular cones are accumulated and averaged over many events. Even though the jet areas of jets, reconstructed with anti-k_{T}, are close to ideal circles (compare Fig. 2.2), the differences in jet area have to be taken into account. Therefore the spectra are weighted for each jet (resolution parameter R) with the ratio of the determined jet area to the ideal circular case ($\pi \cdot \mathrm{R}^2$). This further correction is applied to the variables on a jet-by-jet basis. The z^{ch} variable is calculated from $p_{\mathrm{T}}^{\mathrm{particle,perp}}/p_{\mathrm{T}}^{\mathrm{jet,rec}}$. The radial distributions of p_{T} density are obtained relative to the axis of the perpendicular cone [1].

5.2.1 Implementation of UE corrections in Rivet

Rivet output should only contain the histograms that are presented in the corresponding paper, the UE distributions are therefore filled in temporary histograms. They are deleted after the finalize method. All different types of histograms introduced in section 4.2 were used within this analysis code. For the cross sections and fragmentation distributions standard histograms are used, whereas for averaged

observables such as $\langle N_{ch} \rangle$, $\langle R_{80} \rangle$, $\langle \mathrm{d}p_{\mathrm{T}}^{sum}/\mathrm{d}r \rangle$, profile histograms are the right choice. To subtract two histograms, as needed for the subtraction of the UE fragmentation distributions, a standard YODA function is used.

At this stage of Rivet and YODA development, no such function exists, correctly subtracting two profile histograms. This was taken care of by writing a function that subtracts the y mean in each bin in x of the two profile histograms and filling the obtained value in a scatter plot. The statistical error in each bin is calculated by the quadratic sum of the standard errors of the means.

We would like to point out that the corrected averaged distributions, being saved as scatter plots, can no longer be merged properly. When the YODA merge tool is used, scatter plots are averaged assuming equal run sizes. This does not take into account different weights of individual distributions.

5.3 Generation process

For the real measurement $177 \cdot 10^6$ minimum bias events were analysed. In order to achieve adequate statistics either an even higher number of MB events has to be generated or the generation of higher p_{T} final state partons has to be enhanced.

Since computing time of the generation and the Rivet analysis is quite long[2], the latter option was chosen. A small bias has been introduced, so that the number of generated events can be significantly smaller. It was required that the lowest p_{T} of a hard final state parton (p_{T}-hard) is above 10 GeV/c which drastically increases the number of jets that survive the p_{T} cut of 20 GeV/c. To effectively populate the highest $p_{\mathrm{T}}^{\mathrm{jet,ch}}$ intervals (40 - 60 and 60 - 80 GeV/c), the generation process was repeated with a p_{T}-hard minimum of 30 GeV/c. These requirements ensure that statistics of about $10 \cdot 10^6$ analysed events are already sufficiently high. The p_{T}-hard threshold was chosen low enough to avoid any bias on the observables reported in the respective jet p_{T} intervals.

[2]The evaluation of 100 events takes about 20s. This is rather long for Rivet standards and is ascribed to jet reconstruction with four different resolution parameters and the calculation of the jet areas.

Chapter 6

Results

In this chapter the individual observables are presented and compared to Pythia8 simulations in the respective sections. In section 6.6 the effect of the subtraction of the UE contribution is shown, on the base of a set of selected observables that are most sensible to UE contribution.

Jet reconstruction within Rivet is based on MC particles that are assigned with their true mass. The jet reconstruction in ALICE, however, is based on particles, with masses set to zero. The resulting difference in the jet reconstruction will in the following be referred to as mass effect. The mass effect is explained in section 6.7 and its impact on the reported observables is presented.

In all figures presented in this chapter, ALICE data points[1], shown in black, correspond to measurements in pp collisions at $\sqrt{s} = 7$ TeV. Black vertical error bars show the quadratic sum of statistical and systematic uncertainties on the data. The results of the measurement are compared to two tunes of Pythia8: 4C (red) and MONASH (blue). Statistical uncertainties of the simulations are displayed as vertical error bars. In the bottom panels the ratios of Monte Carlo results to data are shown, i.e. data is drawn at unity. For the ratios, the total uncertainty on the data is shown as a grey error band. If not stated otherwise the original version of Rivet is used. For the figures shown in section 6.7, a modified, non official version of Rivet is used.

6.1 Inclusive differential charged jet cross sections

In the top panels of Fig. 6.1 the inclusive differential charged jet cross sections are shown for R = 0.4 (left) and R = 0.6 (right). These observables are shown without subtraction of UE contribution.

Both 4C and MONASH strongly deviate from data. The entire spectrum is shifted to the right, i.e. the spectrum in the simulation is harder than observed in the measurement. In the low-p_{T} range, the measured data is most overestimated. The observed discrepancy for tune 4C is worse than for MONASH. Fluctuations in the ratio are dominated by statistical uncertainties of the data. Above 30 GeV/c, despite

[1] The data points are taken from the HepData webpage [48]. A slight modification has been applied to the original file. Bin widths had to be specified manually, because of a submitting problem leading to zero bin widths.

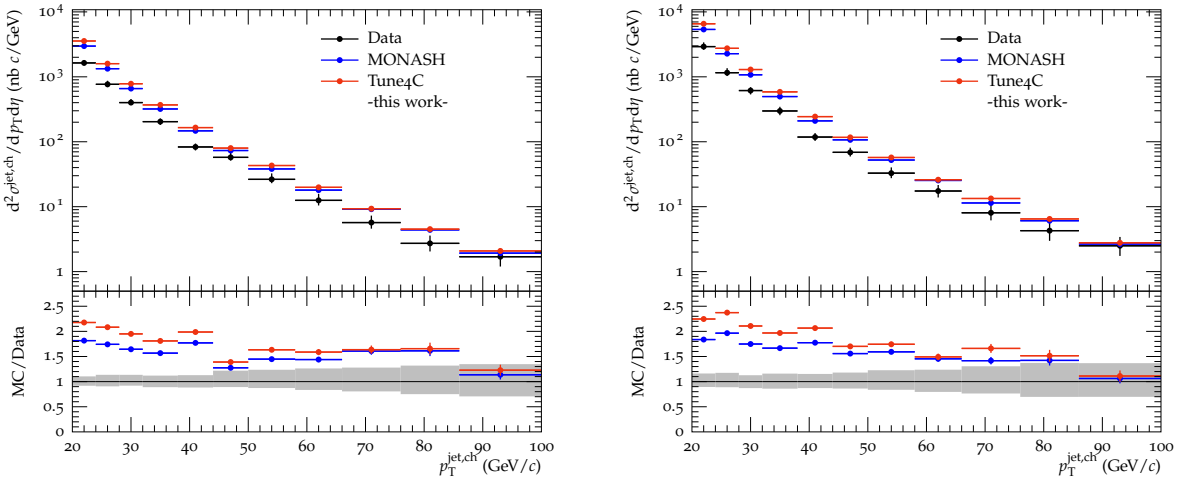

(a) R = 0.4 (b) R = 0.6

Figure 6.1: Inclusive differential charged jet cross sections

the fluctuations, the shape of the spectrum is described rather well over two orders of magnitude.

At low $p_T^{jet,ch}$ a similar trend in the ratios was also observed for Pythia6 (Perugia-0, Perugia-2011 and AMBT1) in [1], yet with smaller discrepancies. The corresponding figure can be found in the appendix A.1.

At high $p_T^{jet,ch}$, Pythia8 simulations deviate from data by a factor of ∼1.5. A deviation of this extent is not yet understood and is therefore objective of further investigation. Simple tests allow to exclude the following reasons for this deviation: merging of multiple runs, the p_T-hard minimum or wrong implementation of kinematic cuts, leading to larger η windows that would increase the jet cross section. In the course of our investigations the mass effect (see section 6.7) on the simulated cross sections was found to be non-negligible, yet does not account for the discrepancy observed in this work. Comparison to event generators, that were used for the original comparison in [1], will shed light on whether this is a Rivet implementation or Pythia8 related deviation.

6.2 Charged particle multiplicity

Figure 6.2 shows the mean charged particle multiplicity distributions as a function of $p_T^{jet,ch}$. Only leading jets are taken into account. The measurement is performed for R = 0.2, R = 0.4, and R = 0.6. The results are presented without subtraction of UE contribution.

In each distribution a monotonic increase with $p_T^{jet,ch}$ is observed. This result corresponds to the picture that initial partons with higher energies can undergo the branching process more often, before the hadronization scale is reached. This leads

to a larger number of final state hadrons, observed as higher jet multiplicities. The average multiplicity also rises with increasing size of the jet cone. The measured average number of jet constituents ranges from 4.5 (smallest value for R = 0.2) to 15 (largest value for R = 0.6). The difference between both Pythia8 tunes is not significant. Since this is the case for all other intra jet observables presented in this chapter, we will in the following refer to both tunes simply as Pythia8. Pythia8 overestimates the jet multiplicities. The absolute deviation is greater for larger cone sizes. The increase with R of the multiplicity leads to similar relative deviations for all three resolution parameters. Pythia8 predictions show a deviation of less than ∼20%, despite two larger deviations at large $p_{\mathrm{T}}^{\mathrm{jet,ch}}$.

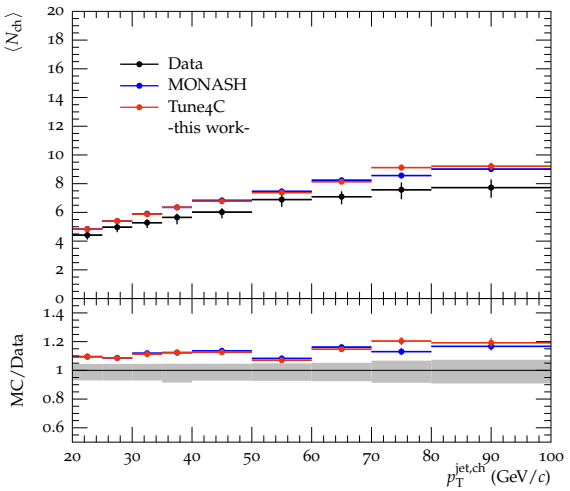

(a) R = 0.2

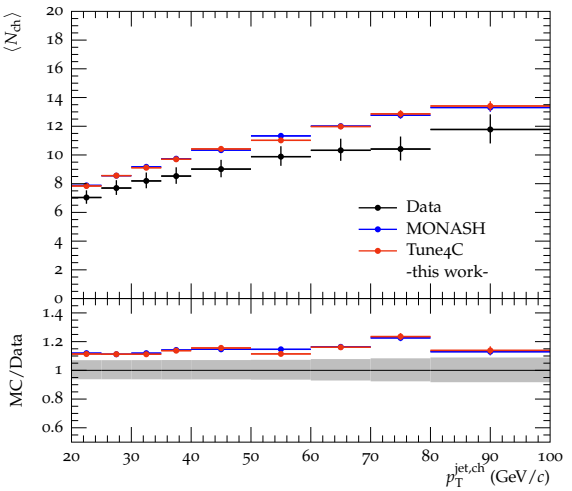

(b) R = 0.4

Figure 6.2: Mean charged particle multiplicity

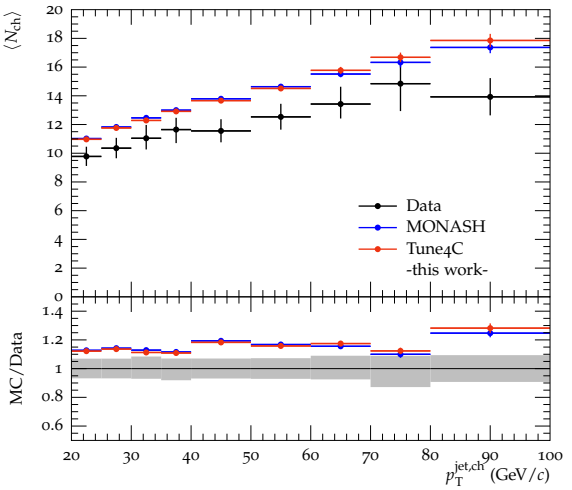

(a) R = 0.6

6.3 Charged jet size

Figure 6.3 shows the distributions of average radius $\langle R_{80} \rangle$ containing 80% of the total jet p_{T} within the leading jet. The results are presented for the resolution parameters R = 0.2, R = 0.4 and R = 0.6. The average size of jets is largest for low $p_{\mathrm{T}}^{\mathrm{jet,ch}}$. A monotonic decrease with jet p_{T} is observed. This leads to the conclusion, that high-p_{T} jets are more collimated.

A reasonably good agreement between the predictions of Pythia8 and the data is observed for all resolution parameters. Most MC points agree within uncertainties on the data. The average radii are systematically overestimated by Pythia8 by ∼10%, i.e. Pythia8 jets are less collimated.The observable $\langle R_{80} \rangle$ is not a very precise way to determine the spatial extent of jets. The measurement of p_{T} density provides a more differential representation of the jet shape.

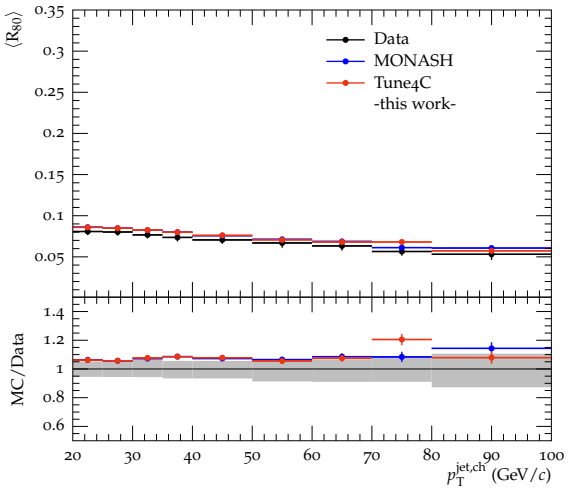

(a) R = 0.2

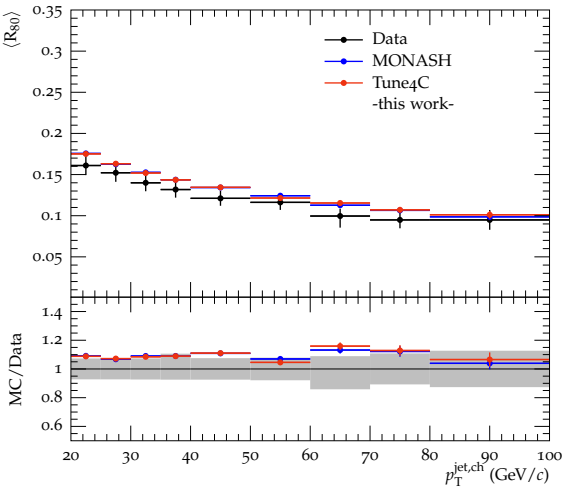

(b) R = 0.4

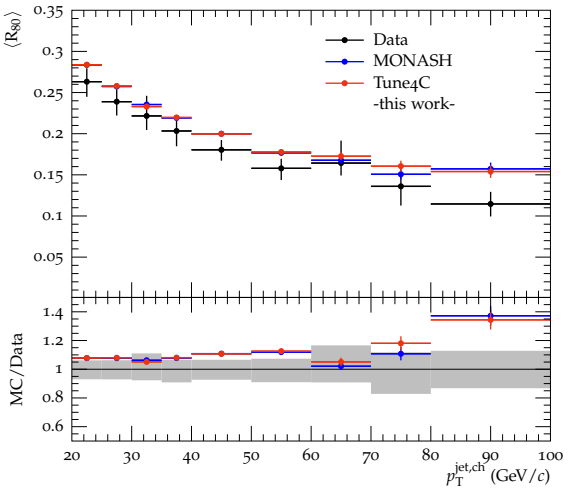

(a) R = 0.6

Figure 6.3: Distributions of average radius R_{80} containing 80% of jet p_{T}

6.4 Transverse momentum density distributions

In this section, we present the average transverse momentum density (p_{T} density) distributions in leading jets, as a function of radial distance 'r' from the jet axis. In Fig. 6.4 (left) and (right) the distributions for jets, reconstructed with R = 0.4 in the p_{T} ranges $20 < p_{\mathrm{T}}^{\mathrm{jet,ch}} < 30$ GeV/c and $60 < p_{\mathrm{T}}^{\mathrm{jet,ch}} < 80$ GeV/c, are shown as examples. The measurement is performed for jets with R = 0.2, R = 0.4 and R = 0.6 for four bins of jet p_{T}, respectively. To emphasize the differences of increasing jet p_{T}, the lowest and highest jet p_{T} intervals are presented here. The intermediate ones show a similar behaviour, as do all the p_{T} density distributions obtained for the different cone sizes.

The p_{T} density is largest near the jet axis and decreases strongly with increasing distance r. As expected, the overall p_{T} density is larger in jets with higher jet p_{T}. The values of p_{T} density decrease by one (left) and two (right) orders of magnitude within the radius R. The slope is steeper for the higher jet p_{T}. This indicates a stronger collimation of highly energetic jets compared to jets with lower energies. This is consistent with the $p_{\mathrm{T}}^{\mathrm{jet,ch}}$ dependence of R_{80}.

A small dip is observed for the lowest radius interval in Fig. 6.4 (left). The distributions are not corrected for the increase of the annular areas, with increasing distance. The fact that the dip is only observed for the lower jet p_{T} interval, indicates that less energetic jets are more diffuse in the central region. This is consistent with the observation that they are in general less collimated.

The comparison to Pythia8 shows an agreement within uncertainties for small distances. There is no significant difference between tune 4C and MONASH. A clear dependence of the ratio on r is observed, indicating that Pythia8 underestimates the p_{T} density at small radii, shifting it to the outer areas of the jet cone. This tendency is observed for all jet p_{T} intervals and resolution parameters to a similar extent. This implies that jets predicted by Pythia8 are less collimated. This is consistent with larger average radii of Pythia8 jets as observed in the previous section.

The MC results shown in Fig. 6.4 (right) are obtained from the evaluation of Pythia8 events with a p_{T}-hard minimum of 30 GeV/c. This is not expected to have an effect on the shape of jets with a p_{T} above 60 GeV/c.

6.5 Jet fragmentation

A set of the measured fragmentation distributions $F^{p_{\mathrm{T}}}$, F^{z} and F^{ξ} without the subtraction of UE contribution is presented in Fig. 6.5. The measurement was solely performed for leading jets with resolution parameter R = 0.4 for four different intervals of jet p_{T}. Only two intervals (20 - 30 and 40 - 60 GeV/c) are shown respectively for each distribution, since no significant overall deviations were observed for the other intervals.

Figures 6.5 (top-left) and (top-right) show the charged particle p_{T} spectra. These spectra span two to three orders of magnitude, showing a monotonic decrease. The

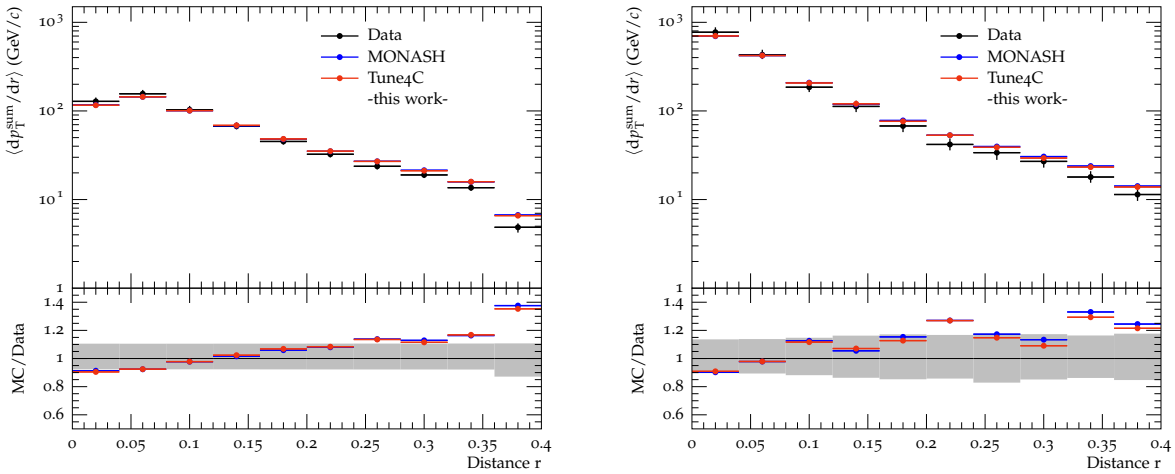

(a) 20 < jet p_{T} < 30 GeV/c (b) 60 < jet p_{T} < 80 GeV/c

Figure 6.4: Distribution of p_{T} density as a function of radial distance r from the jet axis for R = 0.4

dependence on $p_{\mathrm{T}}^{\mathrm{particle}}$ is stronger for small particle p_{T}, i.e. the spectra are steeper and flatten with larger particle p_{T}. This is driven by the jet energy scale. For the scaled particle transverse momentum $z > 0.1$, all the measured distributions for the four different jet p_{T} intervals agree within uncertainties. This indicates a scaling of charged jet fragmentation with charged jet transverse momentum.

The scaled p_{T} spectra F^{ξ} shown in Fig. 6.5 (bottom-left) and (bottom-right) emphasize the fragmentation into low p_{T} particles. High (low) values of ξ correspond to low (high) p_{T} particles. A clear maximum is observed at ξ values between 2 and 3, corresponding to particle $p_{\mathrm{T}} \sim 2$ to 5% of the total jet p_{T}. This maximum is often referred to as "humped-back plateau". The decrease in F^{ξ} to higher values of ξ indicates the suppression of soft particle production due to QCD coherence effects [49, 50]. The significant deviations of the Pythia8 predictions from data show the same deviation tendency for all intervals of jet p_{T}. Pythia8 predicts an amount of low-p_{T} particles (0 - 4 GeV/c) within jets that lies 20% above the measured value, whereas the amount of highly energetic particles is underestimated. The scaling behaviour is clearly observable for the Pythia8 tunes.

6.6 Underlying event subtraction

This section presents the effects of corrections for UE contribution on the observables. The UE contribution dominates at low particle p_{T}. Observables that are sensible to changes of the soft particle yield are therefore affected most. This includes the mean

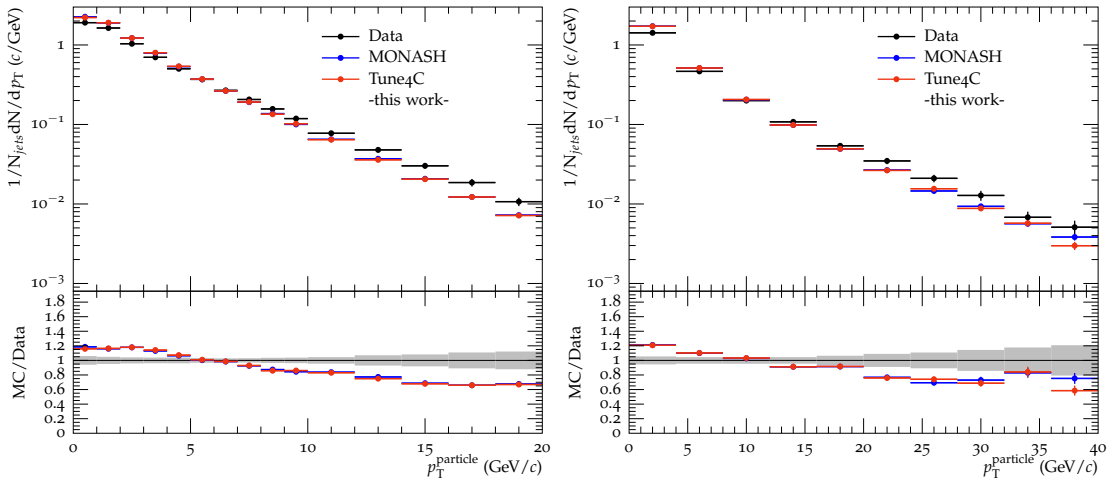

(a) F^{p_T} with $20 <$ jet $p_T < 30$ GeV/c (b) F^{p_T} with $40 <$ jet $p_T < 60$ GeV/c

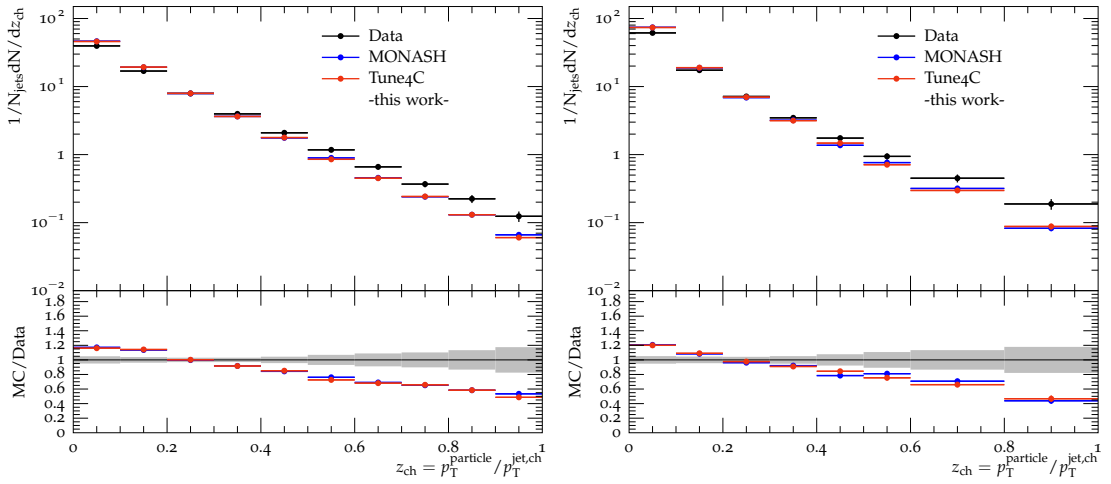

(c) F^z with $20 <$ jet $p_T < 30$ GeV/c (d) F^z with $40 <$ jet $p_T < 60$ GeV/c

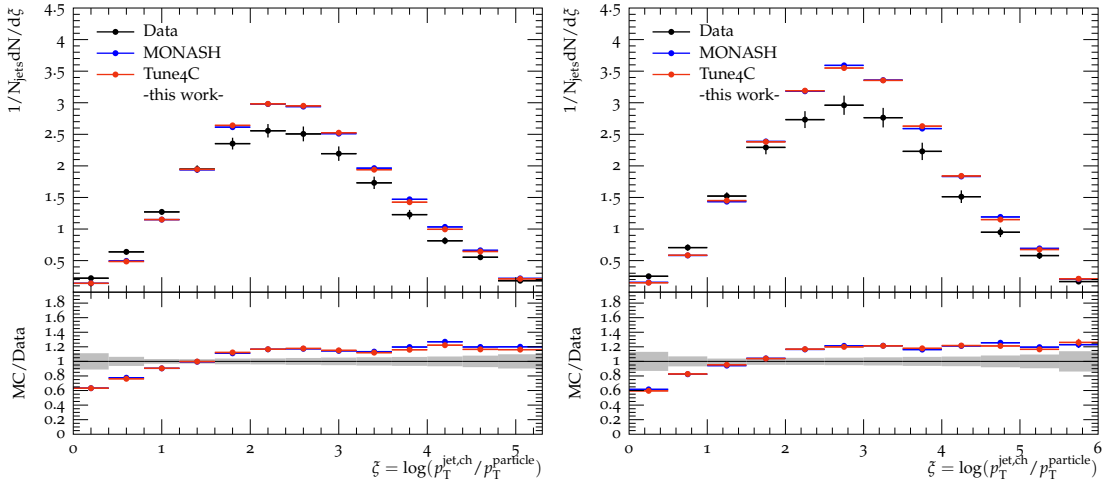

(e) F^ξ with $20 <$ jet $p_T < 30$ GeV/c (f) F^ξ with $40 <$ jet $p_T < 60$ GeV/c

Figure 6.5: Charged particle (scaled) p_T spectra for R = 0.4

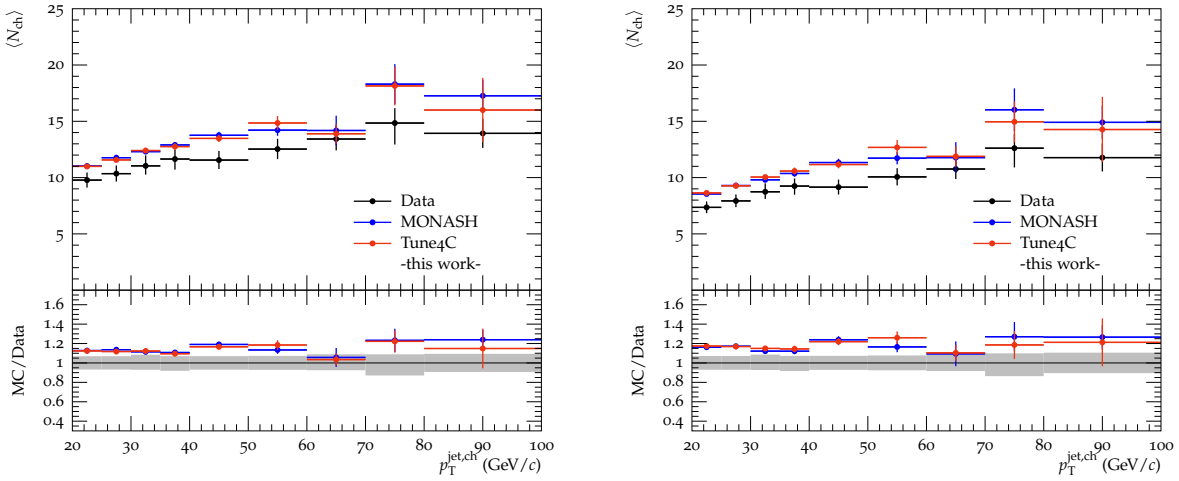

(a) $\langle N_{ch} \rangle$ uncorrected

(b) $\langle N_{ch} \rangle$ with subtraction of UE

Figure 6.6: Mean charged particle multiplicity with and without corrections for UE contribution for R = 0.6

charged particle multiplicities, the p_{T} density[2] and the scaled p_{T} spectrum F^{ξ}, the last two measured in the lowest jet p_{T} interval.

The most fundamental observable related to jet studies are cross sections. The effect of the UE subtraction is small, of the order of a few percent at $p_{\mathrm{T}}^{\mathrm{jet,ch}} = 22$ GeV/c. For completeness, the corrected cross sections are shown in the appendix A.2 for all four resolution parameters R = 0.2, R = 0.3, R = 0.4 and R = 0.6. The discrepancy, between Pythia8 predictions and data, increases with increasing resolution parameter. For small $p_{\mathrm{T}}^{\mathrm{jet,ch}}$ (< 30 GeV/c) a small improvement in the agreement is observed for both R = 0.4 and R = 0.6. A similar improvement of the agreement, after the UE subtraction, was also observed in [1].

The mean charged particle multiplicity for leading jets with R = 0.6 is shown in Fig. 6.6 both with (right) and without (left) subtraction of UE. The average number of particles per jet that can be assigned to the UE $\langle N_{ch,perp} \rangle$ is distributed quite uniformly over the observed jet p_{T} interval. Table 6.1 lists the $\langle N_{ch,perp} \rangle$ found within the perpendicular cones, for jet p_{T} between 20 and 70 GeV/c (Due to large statistical uncertainties the last two jet p_{T} intervals are omitted). The uncertainties of the mean are given by the standard deviation. The three values agree reasonably well. MONASH shows a better agreement with data and slightly overestimates the UE, whereas it is underestimated by tune 4C. The MC/Data agreement becomes slightly worse after the subtraction of UE. For smaller total values of $\langle N_{ch} \rangle$ the initial deviation, which is not decreased, makes a larger difference. This tendency was

[2]The results that show the effect of the UE subtraction on $\langle N_{ch} \rangle$ and $\langle \mathrm{d}p_{\mathrm{T}}^{sum}/\mathrm{d}r \rangle$ are based on $1 \cdot 10^6$ events that were generated in one process in order to avoid the merging of multiple runs.

Table 6.1: Average particle multiplicity found within the perpendicular cones $\langle N_{ch,perp} \rangle$ for R = 0.6 for $20 < p_{\mathrm{T}}^{\mathrm{jet,ch}} < 70$ GeV/c

	$\langle N_{ch,perp} \rangle$
ALICE	2.44 ± 0.11
MONASH	2.47 ± 0.04
Tune4C	2.24 ± 0.13

observed for all resolution parameters. The contribution of UE increases with cone size, the average UE particle multiplicity for R = 0.4 is approximately 1.

Figure 6.7 shows the p_{T} density distributions for leading jets with R = 0.6 within the range $20 < p_{\mathrm{T}}^{\mathrm{jet,ch}} < 30$ GeV/c with (right) and without (left) subtraction of UE. It is assumed that the UE particles are distributed randomly. The high p_{T}^{sum} close to the jet axis (r < 0.24) is only marginally affected by soft UE particles. For large radial distances from the jet axis, corresponding to larger areas and lower p_{T}^{sum}, the sum of UE particles becomes relevant. A clear drop is observed for the largest radial distance in the data, indicating that most of the p_{T} in the outer cone regions is assigned to UE contribution.

The deviation of MC/Data is slightly increasing for higher r. For the largest distance it deviates significantly. The subtracted $\langle p_{\mathrm{T},perp}^{sum} \rangle$ in this annular region is about 6 GeV/c for both Pythia8 tunes and the data. The huge deviation is thus related to the deviation of the uncorrected distribution. The MONASH $\langle p_{\mathrm{T},perp}^{sum} \rangle$ is higher, than the measured value, whereas it is lower for 4C. Similar observations are made for R = 0.4. Changes in the distributions for R = 0.2 are hardly noticeable.

Putting an emphasis on low p_{T} particles, F^{ξ}, shown in Fig. 6.8, is the observable which is most sensible to UE contribution. The high ξ, i.e. the soft region is affected most. The absolute discrepancy between Pythia8 descriptions and data are smaller after UE subtraction. Both Pythia8 tunes overestimate the UE contribution to the soft particle yield. Whereas the contribution to high p_{T} particle yield is underestimated.

6.7 Mass effect on the jet observables

The distance measure introduced for sequential recombination algorithms (see Equ. 2.1) depends on rapidity y. A smaller particle y leads to smaller distances d_{ij}. Systematically smaller d_{ij} effectively show the effect of a slight increase in R. The rapidity is defined as $y = \frac{1}{2}\, ln(\frac{E+p_{\mathrm{L}}}{E-p_{\mathrm{L}}})$ and therefore depends on the particle mass. The rapidity of a particle with a non vanishing mass is lower than for zero mass particles (y tends to zero for infinite particle mass).

In ALICE jets are reconstructed assuming $E^2 = p^2$, i.e. the masses of the particles are set to zero. Since no particle identification is used in the jet reconstruction, this

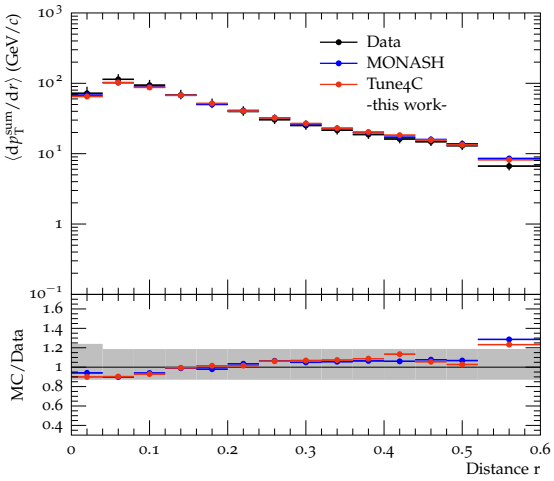

(a) $\langle \mathrm{d}p_{\mathrm{T}}^{sum}/\mathrm{d}r \rangle$ uncorrected

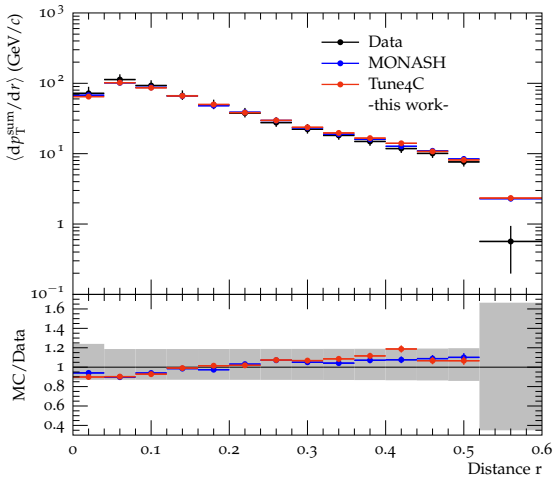

(b) $\langle \mathrm{d}p_{\mathrm{T}}^{sum}/\mathrm{d}r \rangle$ with subtraction of UE

Figure 6.7: Distribution of p_{T} density for 20 < jet p_{T} < 30 GeV/c with and without corrections for UE contribution for R = 0.6

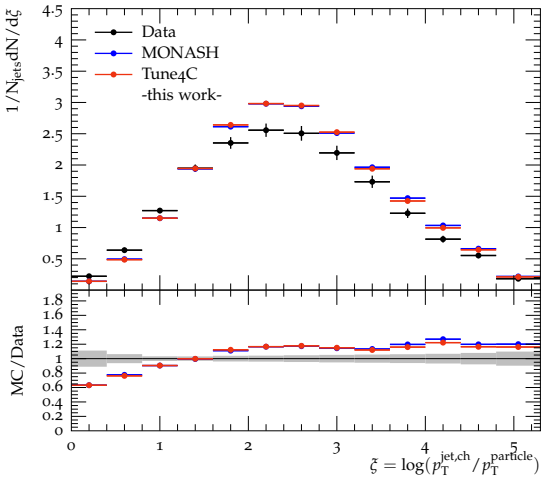

(a) F^{ξ} uncorrected

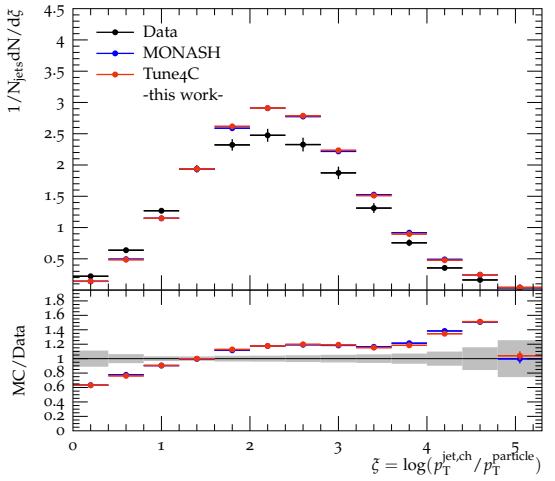

(b) F^{ξ} with subtraction of UE

Figure 6.8: Scaled p_{T} spectrum $\mathrm{d}N/\mathrm{d}\xi^{ch}$ for 20 < jet p_{T} < 30 GeV/c with and without corrections for UE contribution for R = 0.4

is a rather arbitrary choice. No matter what choice is made, it needs to be consistent for both MC and data. Throughout this work we found, that this consistency is not given for the comparison between the Rivet MC and ALICE analysis. In contrast to the original ALICE analysis, where the masses of both measured and MC particles were set to zero, Rivet automatically reconstructs jets, taking into account the true particle masses, as given in the HepMC file.

To show the effect of this inconsistency (the mass effect) on the jet observables the internal Rivet code had to be modified. The particles of the modified Rivet version, 'projected out' by the ChargedFinalState projection, have zero mass, as well and are hence comparable. The figures shown in this section are not based on an official version of Rivet. For clarity reasons, only the MONASH tune is shown. No significant differences in the effect of the modification are observed for 4C. The distributions plotted in green correspond to the modified version of Rivet, labelled with MONASH, modified.

We present a set of observables that showed a non negligible effect. In Fig. 6.10 the effect on the jet observables $\langle N_{ch} \rangle$ and $\langle \mathrm{d}p_{\mathrm{T}}^{sum}/\mathrm{d}r \rangle$ is shown for R = 0.6 and on F^{ξ} ($20 <$ jet $p_{\mathrm{T}} < 30$ GeV/c) for R = 0.4.

As expected, the average charged particle multiplicities are smaller and a better agreement with data is observed. The outermost annular region of the jet is effected most, as indicated by the clear drop in the MONASH p_{T} density for large distances from the jet axis. A significant improvement in the agreement for large distances is observed for all resolution parameters. The low-p_{T} particle yield is significantly smaller and a better agreement of MC/Data is observed for F^{ξ}.

Only small improvement is observed for the cross sections, see Fig. 6.9. For smaller jet p_{T} the modified cross sections are significantly smaller, yet with small absolute discrepancies. For larger p_{T} they are slightly higher, yet in agreement within uncertainties. The effects on R_{80} are not significant.

The mass effect cannot explain the overall discrepancy observed for most of the jet observables. A visible improvement of the overestimated charged particle multiplicity and production of low p_{T} particles, as well as of the p_{T} density distribution is observed. Since the effect is not negligible, the possibility to reconstruct jets based on zero MC particle masses, should be included in the official Rivet versions.

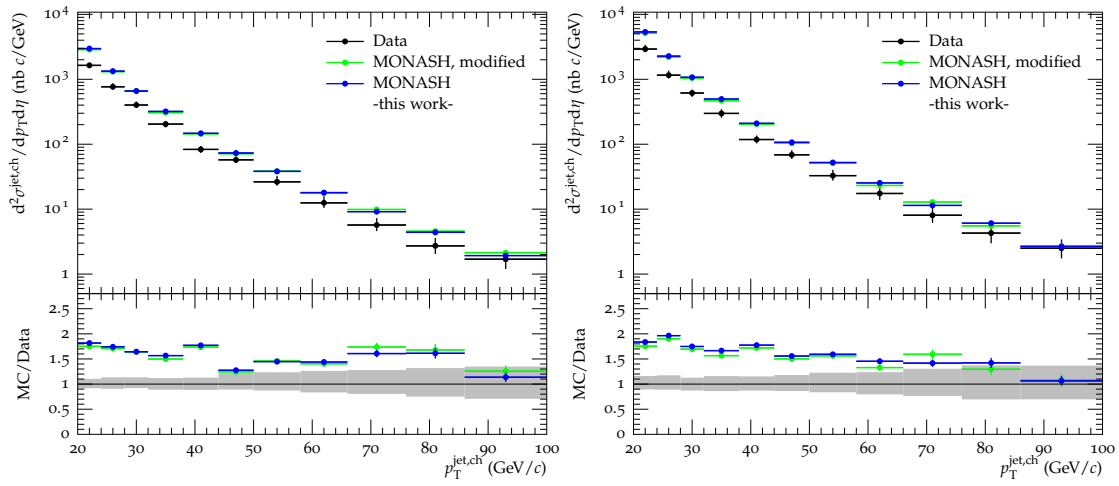

(a) R = 0.4 (b) R = 0.6

Figure 6.9: Impact of the mass effect on the cross sections

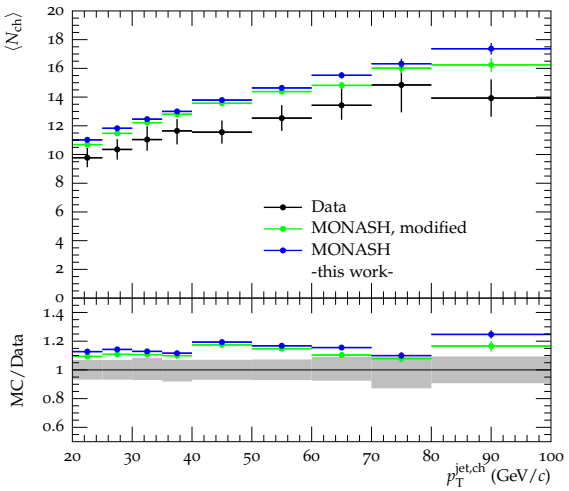

(a) $\langle N_{ch} \rangle$

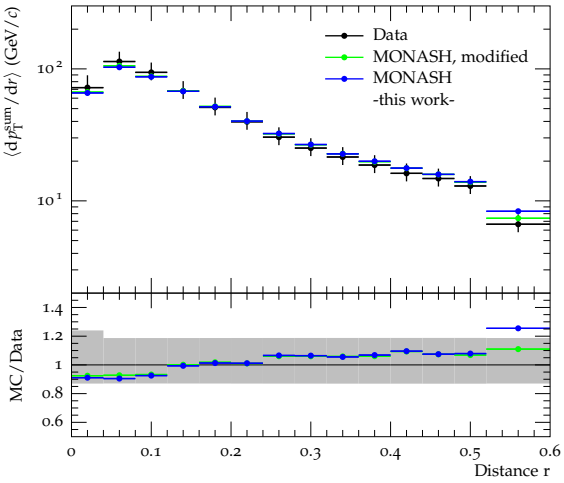

(b) $\langle dp_T^{sum}/dr \rangle$ for 20 < jet p_T < 30 GeV/c

Figure 6.10: Impact of the mass effect on the charged particle multiplicity (R = 0.6), p_T density (R = 0.6) and jet fragmentation (R = 0.4)

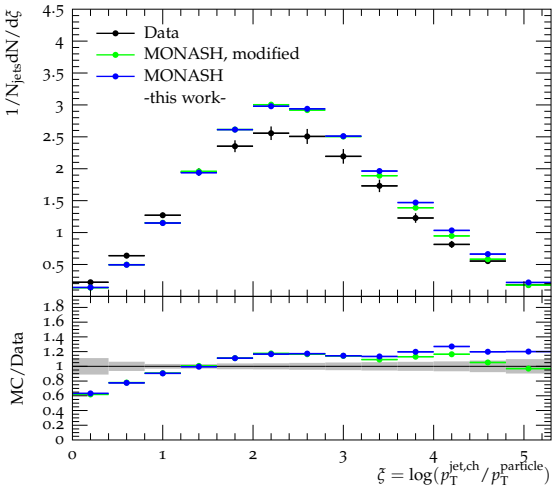

(a) $dN/d\xi^{ch}$ for 20 < jet p_T < 30 GeV/c

Chapter 7

Summary and Outlook

The objective of this work was to implement the ALICE analysis [1], presenting charged jet cross sections and properties in pp-collisions at $\sqrt{s}$ =7 TeV, in Rivet. The analysis comprises the measurement of a set of jet observables, providing detailed information on jet production and jet structure. The different observables are presented both with and without subtraction of UE. All parts of the original analysis have been included in the Rivet analysis.

The implementation in Rivet allows for a comparison of different MC event generators to data. In this thesis a comparison to two tunes of Pythia8 (4C and MONASH) has been carried out.
Pythia8 jet cross sections significantly deviate from the measurements. For lowest $p_{\mathrm{T}}^{\mathrm{jet,ch}}$ (22 GeV/c) the Pythia8 predictions overestimate the measured cross sections by a factor of 1.8 (MONASH) and 2.2 (4C). This large deviation is not yet fully understood and therefore objective to further investigations. A reasonable agreement, however, was found for all other jet observables.

A significant difference between both Pythia8 tunes was only observed for the cross sections. For all other observables they agree within statistical uncertainties. Observed differences in the UE of MONASH and 4C are consistent with observations of the MONASH authors presented in [38].

Throughout this work, we found that jet reconstruction within Rivet is based on MC particles that are assigned with their true mass. The jet reconstruction in ALICE, however, is based on particles, with masses set to zero. The ChargedParticleState projection in Rivet does not yet provide the possibility, to set the masses of MC particles to a certain user defined value. The results obtained with the official Rivet version are therefore, strictly speaking, not comparable to ALICE data. To investigate this mass effect, the Rivet program itself had to be modified. Indeed, a non-negligible impact on the jet observables was found. The Rivet authors will be informed about this, so that this effect will be considered for the next Rivet release.

In order to be validated and become a Rivet built-in analysis, at least one set of MC comparisons carried out in the original analysis, has to be reproduced reasonably well. The observation of the mass effect postponed the required comparison.

The analysis code in its current form, complies with Rivet-coding-style conventions. It will hopefully soon be accepted as a built-in analysis of Rivet, after the required MC comparison and further checks on the cross sections have been carried out.

Appendix A

Additional Figures

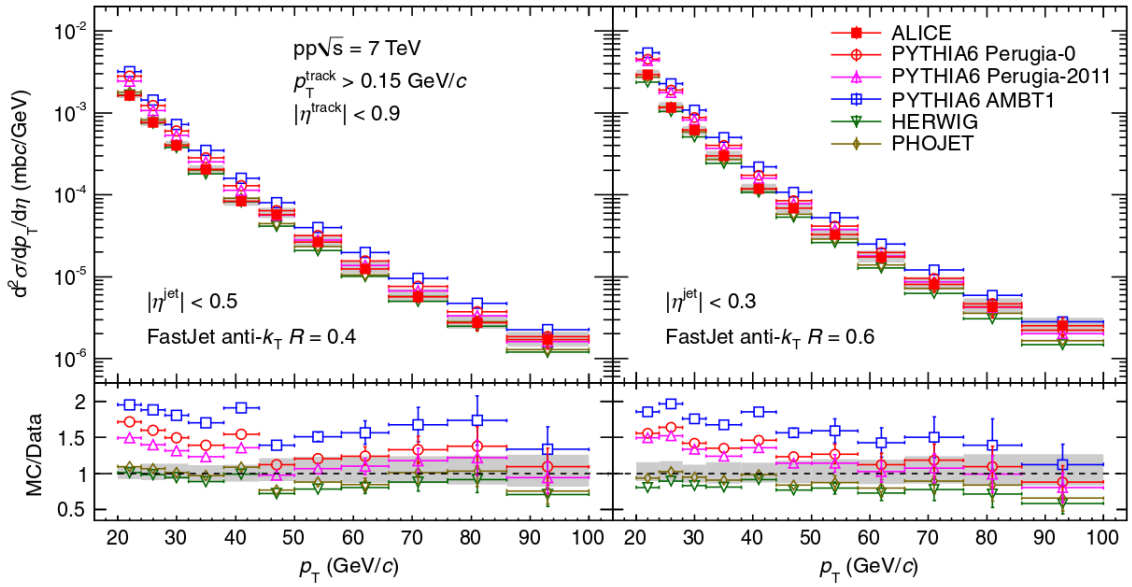

Figure A.1: Top panels: Charged jet cross sections measured in the ALICE experiment in pp collisions at $\sqrt{s} = 7$ TeV without UE subtraction compared to several MC generators: PYTHIA AMBT1, PYTHIA Perugia-0 tune, PYTHIA Perugia-2011 tune, HERWIG, and PHOJET. Bottom panels: Ratios MC/Data. Shaded bands show quadratic sum of statistical and systematic uncertainties on the data drawn at unity. (Fig. 15 in [1])

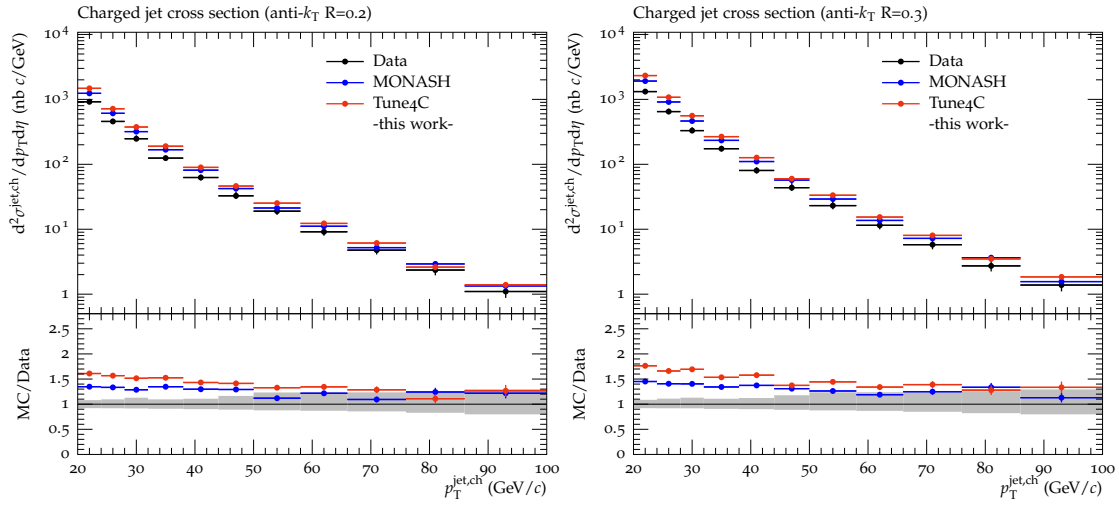

(a) R=0.2 (b) R=0.3

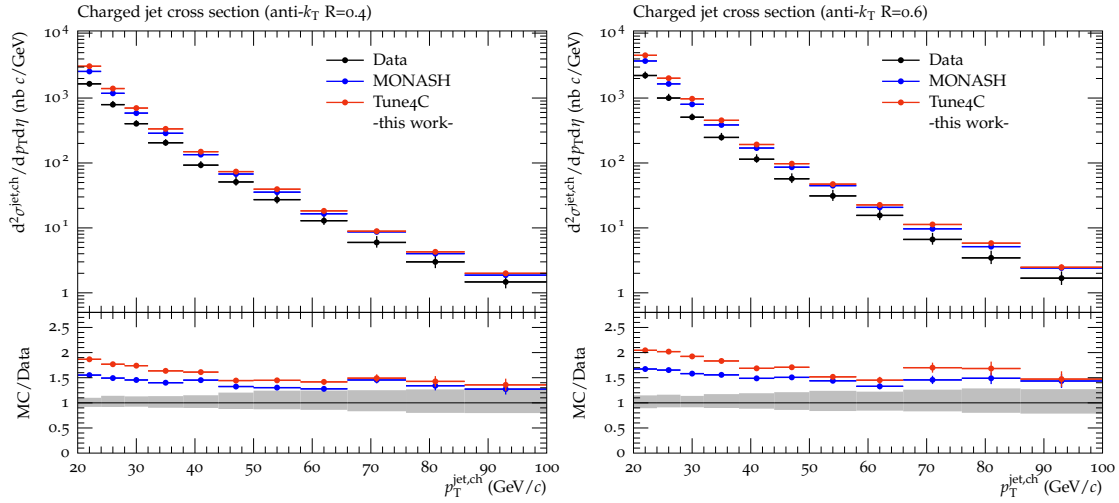

(c) R=0.4 (d) R=0.5

Figure A.2: Inclusive differential charged jet cross sections corrected for UE contribution measured in the ALICE experiment in pp collisions at $\sqrt{s} = 7$ TeV compared to PYTHIA8 (4C and MONASH tune). Bottom panels: Ratios MC/Data. Shaded bands show quadratic sum of statistical and systematic uncertainties on the data drawn at unity.

Appendix B

List of Figures

Appendix C

Bibliography

[1] B. Abelev et al. "Charged jet cross sections and properties in proton-proton collisions at $\sqrt{s} = 7$ TeV". In: *Phys. Rev. D* 91 (11 June 2015), p. 112012. DOI: 10.1103/PhysRevD.91.112012. URL: http://link.aps.org/doi/10.1103/PhysRevD.91.112012.

[2] F. Hinterberger. *Physik der Teilchenbeschleuniger und Ionenoptik*. Springer-Verlag Berlin Heidelberg, 2008.

[3] J. D. Cockcroft and E. T. S. Walton. "Experiments with High Velocity Positive Ions. (I) Further Developments in the Method of Obtaining High Velocity Positive Ions". In: *Proceedings of the Royal Society of London A: Mathematical, Physical and Engineering Sciences* 136.830 (1932), pp. 619–630. ISSN: 0950-1207. DOI: 10.1098/rspa.1932.0107.

[4] M. Thomson. *Modern particle physics*. Cambridge University Press, 2013.

[5] R. Stock. "Relativistic nucleus-nucleus collisions: From the BEVALAC to RHIC". In: *J. Phys.* G30 (2004), S633–S648. DOI: 10.1088/0954-3899/30/8/001. arXiv: nucl-ex/0405007 [nucl-ex].

[6] G. Aad et al. "Observation of a new particle in the search for the Standard Model Higgs boson with the ATLAS detector at the LHC". In: *Phys. Lett.* B716 (2012), pp. 1–29. DOI: 10.1016/j.physletb.2012.08.020. arXiv: 1207.7214 [hep-ex].

[7] S. Chatrchyan et al. "Observation of a new boson at a mass of 125 GeV with the CMS experiment at the LHC". In: *Phys. Lett.* B716 (2012), pp. 30–61. DOI: 10.1016/j.physletb.2012.08.021. arXiv: 1207.7235 [hep-ex].

[8] K. Nakamura and P. D. Group. "Review of Particle Physics". In: *Journal of Physics G: Nuclear and Particle Physics* 37.7A (2010), p. 075021. URL: http://stacks.iop.org/0954-3899/37/i=7A/a=075021.

[9] N. Schmidt. *Neutral Pion Measurements with Conversions in ALICE in pp Collisions at $\sqrt{s}$= 8 TeV*. Dec. 2014. URL: http://www.physi.uni-heidelberg.de//Publications/Bachelorarbeit.pdf.

[10] F. Wilczek. "QCD made simple". In: *Phys. Today* 53N8 (2000), pp. 22–28. DOI: 10.1063/1.1310117.

[11] F. Tkachov. “A contribution to the history of quarks: Boris Struminsky’s 1965 JINR publication”. In: *ArXiv e-prints* (Apr. 2009). arXiv: 0904.0343 [physics.hist-ph].

[12] D. J. Gross and F. Wilczek. “Ultraviolet Behavior of Non-Abelian Gauge Theories”. In: *Phys. Rev. Lett.* 30 (26 June 1973), pp. 1343–1346. DOI: 10.1103/PhysRevLett.30.1343. URL: http://link.aps.org/doi/10.1103/PhysRevLett.30.1343.

[13] H. D. Politzer. “Reliable Perturbative Results for Strong Interactions?” In: *Phys. Rev. Lett.* 30 (1973), pp. 1346–1349. DOI: 10.1103/PhysRevLett.30.1346.

[14] R. P. Feynman. “QED: The Strange Theory of Light and Matter”. In: *Princeton University Press* (1985).

[15] K. Olive and P. D. Group. “Review of Particle Physics”. In: *Chinese Physics C* 38.9 (2014), p. 090001. URL: http://stacks.iop.org/1674-1137/38/i=9/a=090001.

[16] J. W. Harris and B. Muller. “The Search for the quark - gluon plasma”. In: *Ann. Rev. Nucl. Part. Sci.* 46 (1996), pp. 71–107. DOI: 10.1146/annurev.nucl.46.1.71. arXiv: hep-ph/9602235 [hep-ph].

[17] S. Sarkar et al. *The Physics of the Quark-Gluon Plasma*. Springer-Verlag Berlin Heidelberg, 2010.

[18] P. Braun-Munzinger and J. Stachel. “The quest for the quark-gluon plasma”. In: *Nature* 448 (2007), pp. 302–309. DOI: 10.1038/nature06080.

[19] A. Andronic. “The study of quark-gluon matter in high-energy nucleus-nucleus collisions”. In: *AIP Conf. Proc.* 1498 (2012), pp. 125–133. DOI: 10.1063/1.4768487. arXiv: 1210.8126 [nucl-ex].

[20] CERN. *CERN Accelerating science*. http://home.web.cern.ch/about. Aug. 2015.

[21] A. Collaboration. “ALICE: Physics Performance Report, Volume II”. In: *Journal of Physics G: Nuclear and Particle Physics* 32.10 (2006), p. 1295. URL: http://stacks.iop.org/0954-3899/32/i=10/a=001.

[22] B. B. Abelev et al. “Performance of the ALICE Experiment at the CERN LHC”. In: *Int. J. Mod. Phys.* A29 (2014), p. 1430044. DOI: 10.1142/S0217751X14300440. arXiv: 1402.4476 [nucl-ex].

[23] T. Plehn. “Lectures on LHC Physics”. In: *Lect. Notes Phys.* 844 (2012), pp. 1–193. DOI: 10.1007/978-3-642-24040-9. arXiv: 0910.4182 [hep-ph].

[24] B. Andersson et al. “Parton fragmentation and string dynamics”. In: *Physics Reports* 97.2–3 (1983), pp. 31–145. ISSN: 0370-1573. DOI: http://dx.doi.org/10.1016/0370-1573(83)90080-7. URL: http://www.sciencedirect.com/science/article/pii/0370157383900807.

[25] J. D. Bjorken. "Energy Loss of Energetic Partons in Quark - Gluon Plasma: Possible Extinction of High p(t) Jets in Hadron - Hadron Collisions". In: (1982).

[26] S. Collaboration. "Centrality Dependence of High-p_T Hadron Suppression in Au + Au Collisions at $\sqrt{s_{NN}} = 130$ GeV". In: *Phys. Rev. Lett.* 89 (20 Oct. 2002), p. 202301. DOI: 10.1103/PhysRevLett.89.202301. URL: http://link.aps.org/doi/10.1103/PhysRevLett.89.202301.

[27] D. Zaslavsky. *Illustration of jet quenching*. http://www.ellipsix.net/blog/tagged/heavy%20ion%20physics.html. Aug. 2015.

[28] G. P. Salam and G. Soyez. "A Practical Seedless Infrared-Safe Cone jet algorithm". In: *JHEP* 0705 (2007). DOI: 10.1088/1126-6708/2007/05/086. arXiv: 0704.0292 [hep-ph].

[29] M. Cacciari et al. "The Anti-k(t) jet clustering algorithm". In: *JHEP* 0804 (2008). DOI: 10.1088/1126-6708/2008/04/063. arXiv: 0802.1189 [hep-ph].

[30] J. Klein. "Jet Physics with A Large Ion Collider Experiment at the Large Hadron Collider". PhD thesis. Heidelberg U., 2014. URL: http://inspirehep.net/record/1339771/files/CERN-THESIS-2014-186.pdf.

[31] T. Sjostrand et al. "PYTHIA 6.4 Physics and Manual". In: *JHEP* 05 (2006), p. 026. DOI: 10.1088/1126-6708/2006/05/026. arXiv: hep-ph/0603175 [hep-ph].

[32] G. Corcella et al. "HERWIG 6: An Event generator for hadron emission reactions with interfering gluons (including supersymmetric processes)". In: *JHEP* 01 (2001), p. 010. DOI: 10.1088/1126-6708/2001/01/010. arXiv: hep-ph/0011363 [hep-ph].

[33] T. Gleisberg et al. "Event generation with SHERPA 1.1". In: *JHEP* 02 (2009), p. 007. DOI: 10.1088/1126-6708/2009/02/007. arXiv: 0811.4622 [hep-ph].

[34] P. Z. Skands. "Soft-QCD and UE spectra in pp collisions at very high CM energies (a Snowmass white paper)". In: (2013). arXiv: 1308.2813 [hep-ph].

[35] A. Buckley et al. "General-purpose event generators for LHC physics". In: *Phys.Rept.* 504 (2011). DOI: 10.1016/j.physrep.2011.03.005. arXiv: 1101.2599 [hep-ph].

[36] T. Sjostrand et al. "A Brief Introduction to PYTHIA 8.1". In: *Comput. Phys. Commun.* 178 (2008), pp. 852–867. DOI: 10.1016/j.cpc.2008.01.036. arXiv: 0710.3820 [hep-ph].

[37] T. Sjöstrand. *PYTHIA 8 online manual*. http://home.thep.lu.se/~torbjorn/pythia81html/Welcome.html. Aug. 2015.

[38] P. Skands et al. "Tuning PYTHIA 8.1: the Monash 2013 Tune". In: *Eur. Phys. J.* C74.8 (2014), p. 3024. DOI: 10.1140/epjc/s10052-014-3024-y. arXiv: 1404.5630 [hep-ph].

[39] R. Corke and T. Sjostrand. "Interleaved Parton Showers and Tuning Prospects". In: *JHEP* 03 (2011), p. 032. DOI: 10.1007/JHEP03(2011)032. arXiv: 1011.1759 [hep-ph].

[40] A. Buckley et al. "Rivet user manual". In: *Comput.Phys.Commun.* 184 (2013), pp. 2803–2819. DOI: 10.1016/j.cpc.2013.05.021. arXiv: 1003.0694 [hep-ph].

[41] H. Dobbs et al. *HepMC 2 a C++ Event Record for Monte Carlo Generators*. http://lcgapp.cern.ch/project/simu/HepMC/20400/HepMC2_user_manual.pdf. [Online; accessed 27-June-2015]. 2009.

[42] M. Bahr et al. "Herwig++ Physics and Manual". In: *Eur. Phys. J.* C58 (2008), pp. 639–707. DOI: 10.1140/epjc/s10052-008-0798-9. arXiv: 0803.0883 [hep-ph].

[43] H. I. Durham. *AGILe*. https://agile.hepforge.org/. Aug. 2015.

[44] H. I. Durham. *YODA*. https://yoda.hepforge.org/. Aug. 2015.

[45] H. I. Durham. *Rivet*. http://rivet.hepforge.org/. Aug. 2015.

[46] A. Karneyeu et al. "MCPLOTS: a particle physics resource based on volunteer computing". In: *Eur. Phys. J.* C74 (2014), p. 2714. DOI: 10.1140/epjc/s10052-014-2714-9. arXiv: 1306.3436 [hep-ph].

[47] A. Karneyeu et al. *MCplots*. http://mcplots.cern.ch/. Aug. 2015.

[48] D. IPPP. *The Durham HepData Project*. http://hepdata.cedar.ac.uk/reaction. Sept. 2015.

[49] A. Mueller. "On the multiplicity of hadrons in QCD jets". In: *Physics Letters B* 104.2 (1981), pp. 161–164. ISSN: 0370-2693. DOI: http://dx.doi.org/10.1016/0370-2693(81)90581-5. URL: http://www.sciencedirect.com/science/article/pii/0370269381905815.

[50] B. I. Ermolaev and V. S. Fadin. "Log - Log Asymptotic Form of Exclusive Cross-Sections in Quantum Chromodynamics". In: *JETP Lett.* 33 (1981). [Pisma Zh. Eksp. Teor. Fiz.33,285(1981)], pp. 269–272.

Acknowledgements

First and foremost I would like to thank Professor Dr. Johanna Stachel and PD Dr. Klaus Reygers who gave me the opportunity to join the ALICE group and thus the interesting field of particle physics. Since this was my first inclusion into the scientific world, it was really inspiring to work among people who are really dedicated to their work. I would like to thank everyone in the ALICE group for being so welcoming and assisting right from the start. I wish to express my gratitude especially to Oliver Busch for his patience and helpful pieces of advice during my time in this group. Michael Winn has not only continuously offered his help providing both academic and encouraging support, moreover, he gave us bachelor students a broader insight of what is actually going on at CERN. Furthermore, I am indebted to Hans Beck, whom I bothered frequently with server related issues. I also want to thank Sebastian Klewin, who taught me how to work with LateX, and Lukas Layer who patiently helped me, while I was starting to learn programming.

Vielen Dank an alle!

Erklärung:

Ich versichere, dass ich diese Arbeit selbstständig verfasst habe und keine anderen als die angegebenen Quellen und Hilfsmittel benutzt habe.

Heidelberg, den .....